VELA X-1 PULSE TIMING. II. VARIATIONS IN PULSE FREQUENCY

J. E. DEETER AND P. E. BOYNTON[1]
Department of Astronomy, University of Washington

AND

F. K. LAMB[2] AND G. ZYLSTRA[3]
Department of Physics, University of Illinois at Urbana-Champaign
Received 1986 October 30; accepted 1988 May 24

ABSTRACT

This is the second paper reporting our analysis and intepretation of observations of the pulsed X-ray emission from the accretion-powered pulsar Vela X-1. We present the pulse frequency behavior during 1978 May, based on data from *OSO 8*, and during 1978 December–1979 January, based on data from *HEAO 1* and *SAS 3*. The orbital parameters derived in the first paper are used to remove the effect of the neutron star's orbital motion. The frequency record for the time span 1975–1982 is then examined, using previously published frequencies as well as the new ones reported here. From this record it is apparent that there are variations in pulse frequency on all accessible time scales, from 2 days to 2600 days. In particular, the *HEAO 1* observations reveal short-term variations in frequency as rapid as $|\dot{\Omega}/\Omega| = (5.8 \pm 1.4) \times 10^{-3}$ yr^{-1}, with the sign of the derivative reversing on time scales as short as the temporal resolution of the data, which is roughly 2 days. We also construct a power density spectrum of the fluctuations in $\dot{\Omega}$, which covers 13 octaves in analysis frequency. The lower nine octaves of this spectrum are well fitted by a power law with exponent $+0.06 \pm 0.23$, demonstrating that white noise in $\dot{\Omega}$ (a random walk in pulse frequency) is an appropriate description of the pulse frequency fluctuations and the only acceptable simple noise model. The observed strength of the noise is $(8 \pm 2) \times 10^{-19}$ rad^2 s^{-3}. The character of this power density spectrum strongly suggests that the observed variations in pulse frequency on time scales longer than a few days are indeed variations in the rotation rate of the neutron star. The change in the apparent secular trend of the pulse frequency from spin-up to spin-down in 1979 and the frequency variations observed on much shorter time scales are both consistent with white noise in $\dot{\Omega}$ of this strength.

Subject headings: pulsars — stars: neutron — stars: rotation — X-rays: binaries

I. INTRODUCTION

This is the second paper presenting the results of a detailed study of pulse frequency variations in the accretion-powered pulsar Vela X-1. In the first paper (Boynton *et al.* 1986, hereafter Paper I) we described the motivation for this study, the observations, the method used to estimate pulse phases, and the orbital solution we derived from them. There we also reported the presence of stochastic variations in the pulse phase caused by three distinct phenomena: fluctuations in the observed shape of pulses due to the finite number of photons detected, "excess" fluctuations in the pulse shape due to other aspects of the pulse emission process, and additional variations that dominate the frequency record on long time scales. The last phenomenon we associate with irregularities in the rotation rate of the neutron star for reasons discussed below.

In Paper I we showed that the variance in the pulse phase due to excess pulse shape fluctuations could be significantly reduced by applying a filter to the pulse templates prior to the timing analysis. We also showed that for our highest quality data, the uncertainties in the local orbital epoch and the semimajor axis induced by noise in the pulsar rotation rate are larger by factors of 5 and 10 than those attributable to the observed pulse shape fluctuations. Consideration of the rela-

tive importance of these two uncertainties enabled us to weight appropriately five selected orbital solutions in order to construct a *mean orbit* for which the uncertainty in the elements is approximately a minimum.

In the present paper we study in detail the fluctuations in the rotation rate of Vela X-1. The appropriate method for analyzing and interpreting observations of such fluctuations depends on the character of the fluctuations and the structure of the observations. If the fluctuations do not overlap in time and they are resolved with adequate signal-to-noise ratio, the observed pulse frequency time series can be compared directly with deterministic models of the rotation rate as a function of time. If, on the other hand, the fluctuations overlap and/or the observations do not resolve the individual events with adequate signal-to-noise ratio, only the statistical properties of the time series can be determined (for more complete discussions of this problem see Lamb 1977 and Scargle 1982). As discussed below, we appear to be confronted by the latter situation in analyzing currently available X-ray pulse timing observations of Vela X-1. Under these circumstances, the power density spectrum of the fluctuations provides a convenient characterization that can be interpreted relatively easily. Thus, an important goal of the present study is to construct and analyze the power density spectrum of the pulse frequency variations in Vela X-1.

We also explore the possibility of modeling the observed fluctuations in the rotation rate of this star by simple random noise processes (by *simple*, we mean processes with an even integer power-law power density spectrum). The utility of this

376

approach was recognized following the discovery that the small fluctuations observed in the frequency of the rotation-powered pulsar in the Crab nebula can be adequately described by such a process (Boynton *et al.* 1972; Groth 1975). Soon afterwards, Lamb, Pines, and Shaham (1974, 1976) argued on theoretical grounds that the pulse frequency variations seen in many accretion-powered pulsars should also be amenable to a description in terms of simple noise processes and showed that the limited data then available for Her X-1 and Cen X-3 were consistent with this conjecture. Lamb (1977) pointed out that, regardless of its cause, noise in the pulse frequency can be used to probe the internal properties of the pulsing star. These ideas were subsequently worked out in detail by Lamb, Pines, and Shaham (1978*a*, *b*). Motivated by this work, Boynton and Deeter (1979), Boynton (1981), and Deeter (1981) were able, through studies of the observed noise, to place stringent constraints on models of the internal structure of the Crab pulsar and Her X-1. In the case of the Crab pulsar, they specifically ruled out the two-component model proposed by Baym *et al.* (1969) as an adequate description of its full dynamical behavior.

The results presented here depend heavily on a planned sequence of 13 observations made using the *HEAO 1* and *SAS 3* X-ray satellites during 1978 November–1979 January. These observations were spaced to provide approximately one octave resolution over the largest possible range of analysis frequencies, thereby making possible an investigation of at least the coarse features of the power spectrum. These observations, together with previously unpublished *OSO 8* observations from 1978 May, constitute the new data used in both Paper I and the present work. Previously published data have also been used wherever appropriate.

In § II we determine the behavior of the pulse frequency as a function of time. We then construct a representation of these same data in the frequency domain by computing a low-resolution power density spectrum in § III. This spectrum is shown in § IV to be consistent with a simple noise model corresponding to a random walk in the rotation rate of the neutron star.

In § V we argue that the fluctuations in pulse phase that exceed those ascribable to the observed fluctuations in pulse shape are most likely caused by changes in the rotation rate of the stellar crust. Such changes can be produced by the torques acting on the inside and the outside of the crust. The internal torque depends on the state of the interior and its coupling to the crust, whereas the external torque depends on the flow pattern of the accreting plasma. The study of the fluctuations in rotation rate caused by these torques is a particularly promising way to determine the properties of Vela X-1, because stellar rotation is relatively simple in comparison to much other X-ray source physics and has been investigated in detail. Moreover, rotation rates can be determined very precisely with the combined capabilities of modern X-ray detectors and data analysis techniques. Thus, a direct, quantitative confrontation between theory and observation is possible.

Our results have important implications for the structure of the neutron star and the properties of the accretion flow in Vela X-1. A full discussion of these implications will be published elsewhere (Lamb *et al.* 1988). A brief summary of our results has been presented in Boynton *et al.* (1984).

II. PULSE FREQUENCY RECORD

The mean orbit of Vela X-1 derived in Paper I may be used to transform the observed pulse frequency time series to the approximate rest frame of the neutron star. By removing the effects of orbital motion with relatively high precision, the behavior of the pulse emission process and stellar rotation rate is revealed. In this section we describe this behavior as a time history of the pulse frequency.

Even though pulse phase is the fundamental observable in our analysis, a continuous record of phase can be constructed only for those blocks of available data that can be connected by an unambiguous pulse count. In contrast, a compilation of locally determined pulse frequencies can be formed from previously published observations, as well as from our own work. Thus, in order to construct the longest possible record of rotational behavior, we have used locally determined pulse frequencies over time intervals longer than can be connected by an unambiguous pulse count.

We have chosen to report the history of the neutron star's rotation as pulse frequency rather than pulse period largely because of the physical and mathematical simplicity of consistently taking time as the independent variable. Pulse phase is then the dependent variable, and pulse frequency—the time derivative of pulse phase—is the natural measure of pulse rate. For similar reasons, the physics of rotating bodies is couched in terms of rotation frequency, not period. This custom is built into the descriptive language as well: pulsar spin-up and spin-down are awkwardly presented in terms of pulse period because the period goes down during episodes of spin-up and *vice versa*.

In analyzing our own pulse timing data, we begin with the time series of locally estimated pulse phases derived in Paper I. After transforming approximately to the neutron star rest frame using our mean orbit, the pulse phases derived from the 1978 May (*OSO 8*) and 1978 November–1979 January (*HEAO 1, SAS 3*) data sets were converted to a series of pulse frequencies.

Seven frequency estimates were derived from the 1978 May data by dividing the set into seven approximately equal subsets, each of three to five days' duration, and by determining the frequencies as slopes from least-squares straight-line fits to each subset of phases. The duration of the subsets was chosen as small as possible, consistent with the requirement that the uncertainty in each frequency estimate be smaller than the typical change between estimates.

Thirteen frequency estimates were derived from the 1978 November–1979 January data set. Each of these (except the final one based solely on *SAS 3* data) is calculated as a mean frequency for the interval between two consecutive 12 hour observations by first dividing the data from each separate observation into two equal parts, and then fitting a straight line to the pulse phase data from the second half of one observation and the first half of the next. Data from the last half of the final *HEAO 1* pointing was grouped with data from the first day of the 4.5 day *SAS 3* observation, and an additional frequency estimate was computed by fitting a straight line to the final 3.5 days of the *SAS 3* data. Because of the relative sparseness of the *HEAO 1* and *SAS 3* data, the resulting frequency record is not nearly as uniform as the record from the *OSO 8* data. We also computed frequencies based solely on the data *within* each *HEAO 1* pointing. These "within" frequencies were consistent with the "between" frequencies, but otherwise add nothing to the representation because of their relatively large uncertainties. They are not considered further in the present analysis.

The uncertainties in the frequency estimates are affected by all three noise sources mentioned in § I. The combined effect of

DEETER *ET AL.*

the two types of fluctuation in pulse shape is found to dominate the uncertainty in pulse phase for time intervals over which phase estimates are computed (0.04–0.5 days). Both types of fluctuation produce statistically independent fluctuations in phase and consequently yield white noise in that variable. For this reason, in the remainder of this discussion we refer to them jointly, as "pulse shape noise." The estimated rms uncertainties, nominally 0.51, 0.7, and 1.32 s, respectively, for the individual *HEAO 1*, *SAS 3*, and *OSO 8* phases (see Paper I), may be propagated into the frequency estimates to yield appropriate frequency uncertainties. The frequency estimates and their uncertainties due to pulse shape noise alone are listed in Table 1 and plotted in Figure 1. Uncertainties calculated in this way fully characterize the pulse frequency estimates made in the satellite observing frame or any other frame with a relative motion that is precisely specified, such as the Solar System barycenter.

The motion of the frame of interest, namely that of the neutron star, is not known precisely, and this introduces an additional uncertainty in the pulse frequency, when calculated in the frame of the neutron star. The reason is that the inaccuracy of the orbital elements and consequent error in the calculated motion of the source frame produces a corresponding variation in the pulse frequency time series when transformed to that nominal frame. The resulting contribution to the uncertainty in pulse frequency would exist even if pulse shape noise

was the only noise present. But in practice, the red noise components in the pulse phase fluctuation spectrum of Vela X-1 completely dominates the white noise component at the orbital frequency ($\sim [9 \text{ days}]^{-1}$), and makes determinations of the orbit of Vela X-1 by pulse timing much more uncertain. This uncertainty is unavoidable as long as pulse timing remains the most precise method of determining the neutron star orbit.

To see the effect of the orbital uncertainty on the frequency record, consider the simplified situation of a circular orbit. For a frequency estimate calculated from a phase difference measured over a time interval, Δt, the uncertainty contributed by the orbit is shown in the Appendix to be

$$\sigma_\Omega = \Omega_{\text{orb}} \, \sigma_x \, | \operatorname{sinc} \tfrac{1}{2} \Omega_{\text{orb}} \Delta t | , \qquad (1)$$

where σ_x is the uncertainty in $x = (\Omega a/c) \sin i$, the projected semimajor axis, measured in units of pulse phase. If the orbit is not circular, it is necessary to add a second error term similar to that of equation (1), but with Ω_{orb} replaced by $2\Omega_{\text{orb}}$.

The uncertainty computed in this way is adequate for discussing a single frequency estimate, but a complication arises if two or more frequency (or phase) estimates are to be compared. In general the errors of all such estimates will be correlated except those computed using time intervals equal to integer multiples of the orbital period, for which the variance and any covariance contribution vanishes. For a circular orbit,

TABLE 1

New Pulse Periods and Frequencies for Vela X-1, Showing Effect of Uncertainty in Orbital Parameters

T_{mid} (JD $-2,440,000$)	Span (days)	Pulse Period[a] (s)	Pulse Frequency[b] (mrad s^{-1})	$\Delta\Omega$[c] (nrads s^{-1})					Weight[d]
				Σ	$T_{\pi/2}$	x	e	ω	
1978 May									
3640.01	3.18	282.80452 (169)	22.217415 (133)	76	-15	65	-37	-2	0.14
3645.62	3.65	282.80016 (127)	22.217757 (100)	75	-40	-57	6	-25	0.14
3651.04	5.15	282.79188 (88)	22.218408 (69)	50	49	13	0	3	0.14
3656.02	3.79	282.78806 (127)	22.218708 (100)	66	-60	2	23	12	0.14
3660.75	4.66	282.78884 (99)	22.218647 (78)	55	54	-6	5	4	0.14
3665.47	3.70	282.78899 (127)	22.218635 (100)	65	-56	24	8	23	0.14
3669.99	4.30	282.79104 (110)	22.218474 (86)	61	57	-19	7	9	0.14
1978 November–1979 January									
3825.78	23.50	282.74884 (5)	22.221790 (4)	10	-9	-4	-2	1	0.13
3840.43	5.66	282.74606 (27)	22.222008 (21)	38	31	-18	-1	-13	0.13
3846.77	6.88	282.75233 (20)	22.221516 (16)	30	6	26	9	11	0.13
3853.10	5.66	282.75604 (19)	22.221224 (15)	42	-40	-6	-12	-4	0.13
3857.59	3.18	282.75640 (37)	22.221196 (29)	72	66	9	28	6	0.13
3859.94	1.40	282.75881 (87)	22.221006 (68)	109	-5	-88	-57	-31	0.13
3861.38	1.34	282.75240 (108)	22.221510 (85)	105	-71	-39	59	-31	0.13
3862.75	1.28	282.74948 (94)	22.221740 (74)	87	-61	33	7	53	0.13
3864.21	1.52	282.75004 (68)	22.221696 (53)	97	-13	75	-60	-6	0.13
3866.59	3.12	282.74616 (29)	22.222000 (23)	76	68	8	31	9	0.13
3871.00	5.60	282.75346 (21)	22.221427 (17)	42	-40	-6	-11	-4	0.13
3881.64	15.56	282.74632 (14)	22.221988 (11)	14	7	-10	5	-4	0.13
3891.30	2.50	282.75020 (88)	22.221683 (69)	88	-6	72	-48	-16	0.13

[a] Pulse period with respect to the mean orbit of Boynton *et al.* 1986. The 1 σ uncertainty in the final decimal place, due to noise in pulse shape, is given in parentheses to the right of each estimate.

[b] Pulse frequency (Ω) with respect to the mean orbit of Boynton *et al.* 1986. The 1 σ uncertainty in the final decimal place, due to noise in pulse shape, is given in parenthesis to the right of each estimate. The unit for this uncertainty is effectively nrads s^{-1}, the same as that for the next five columns, so all six columns can be directly intercompared.

[c] Estimated contribution to uncertainty in pulse frequency ($\Delta\Omega$) due to the uncertainty in the orbital parameters. The column labeled Σ gives the combined uncertainty obtained as the square root of the sum of squares of the entries in the next four columns. The remaining columns give in order the changes in frequency induced by $+1$ σ changes in the mean orbital epoch $T_{\pi/2}$, the projected semimajor axis $x = (a/c) \sin i$, the eccentricity e, and the longitude of periapse ω, respectively.

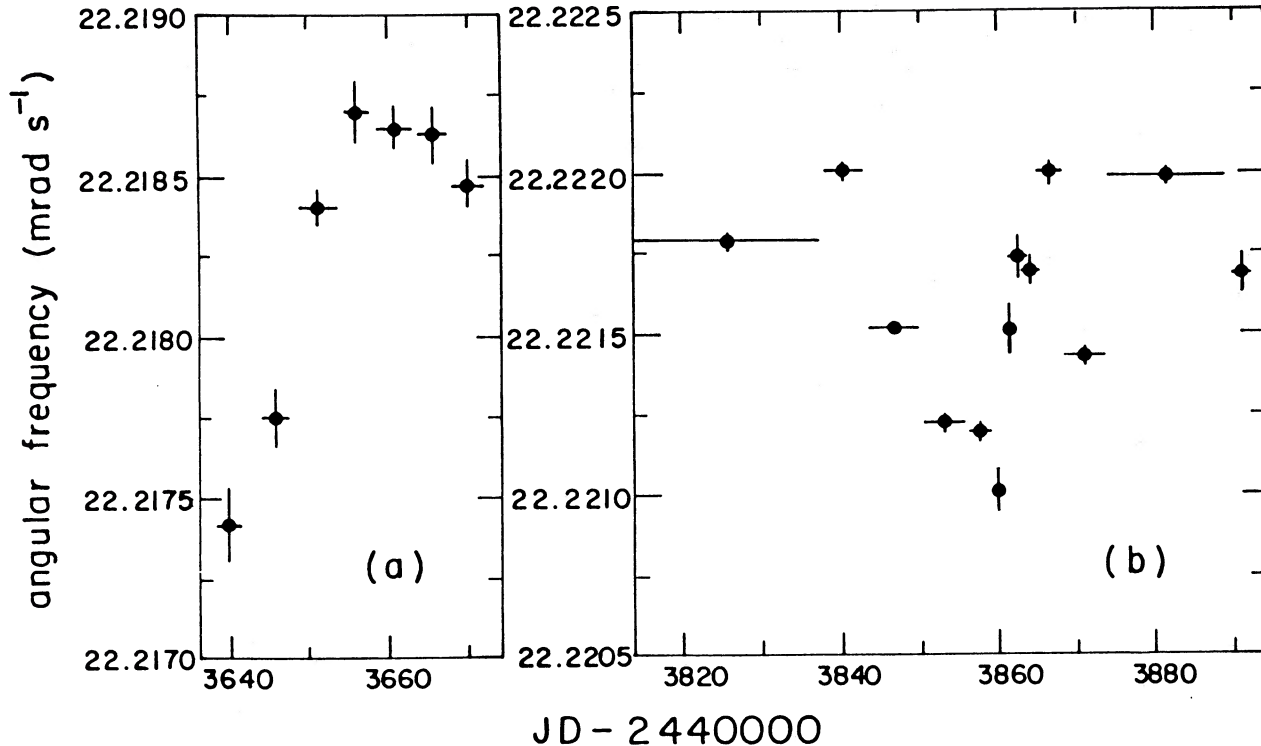[d] Weight used in computing the portion of power spectrum based on pulse frequencies.

FIG. 1.—Short-term history of the angular frequency of Vela X-1, based on the new data presented in Table 1. Vertical bars represent 1 σ confidence intervals. (a) 1978 May, based on *OSO 8* observations. (b) 1978 November–1979 January, based on *HEAO 1* and *SAS 3* observations.

the correlation between any two frequency estimates with mid-times t_1 and t_2 depends on the separation $t_2 - t_1$ as

$$\sigma_{12} = \sigma_1\sigma_2 \cos\left[\Omega_{orb}(t_2 - t_1)\right], \qquad (2)$$

where σ_1 and σ_2 are the uncertainties in each of the two pulse frequencies given by equation (1).

For the haphazard orbital sampling in the data at hand, the variances and covariances are comparable, tedious to calculate in detail, and defy any simple representation in displays of the pulse frequency record. We have therefore chosen to represent this correlated error component in the following way. The effect of the orbital uncertainty on each frequency listed in Table 1 is estimated by computing the change induced by a 1 σ change in each of four orbital parameters: the epoch $T_{\pi/2}$, the semimajor axis x, the eccentricity e, and the longitude of periapsis ω. These four parameters are free from large correlations, so the combined contribution to the error in the frequency can be estimated by taking the square root of the sum of squares of the changes induced by the 1 σ alterations in the four parameters. The combined frequency error is listed in Table 1, together with the individual changes obtained by varying the four parameters. The correlations *between* the frequency estimates due to orbital uncertainties are more difficult to present, but they can be recovered numerically by applying the extension of equation (2) that describes an elliptical orbit.

Table 1 reveals that the uncertainty in the pulse frequency caused by the uncertainty in the orbit is comparable to (*OSO 8*) or greater than (*HEAO 1*) that caused by the pulse shape noise. Nevertheless, the pulse frequency record displayed in Figure 1 shows clearly that the overall uncertainty in the frequency record is much smaller than the observed fluctuations. Consequently, the issue of correlated errors is important only in providing correct uncertainties for derived quantities such

as the local angular acceleration. The situation confronted in analyzing the *HEAO 1* data on Vela X-1 is unfamiliar because the uncertainty in the pulse frequency record is determined more by the uncertainty in orbital elements than by the uncertainty in pulse phase. As mentioned earlier, this is because the power density spectrum of the red noise component dominates the white-noise component at the orbital frequency.

Figure 1 shows that Vela X-1 undergoes statistically significant short-term angular accelerations of both signs, with reversals occurring on the shortest time scales accessible to this study, roughly 2 days. The largest rate of change is found between the frequency estimates centered on JD 2,443,859.94 and 861.38, and corresponds to a relative acceleration $\dot{\Omega}/\Omega = (5.8 \pm 1.4) \times 10^{-3}$ yr^{-1}.

The available pulse frequency estimates are shown in Figure 2, including those based on the previously published data listed in Table 2. The most notable feature in this 8 yr history is an apparent change in spin rate in 1979. This feature and its interpretation are discussed in § IV*b*.

III. CONSTRUCTION OF THE POWER SPECTRUM

We have already suggested in § I that a straightforward approach to the statistical description of the fluctuations observed in the Vela X-1 pulse frequency and/or phase time series is provided by comparison of the power spectrum of the fluctuations with power-law power spectra. Such spectra not only provide a range of simple mathematical models, but are also the type of spectra predicted by a class of simple physical models for the torque acting on the neutron star crust. The stochastic component of such torques may be treated as arising from processes describable as various integrals of white noise and consequently are characterized by power-law spectra with various even integer exponents (Lamb, Pines, and Shaham
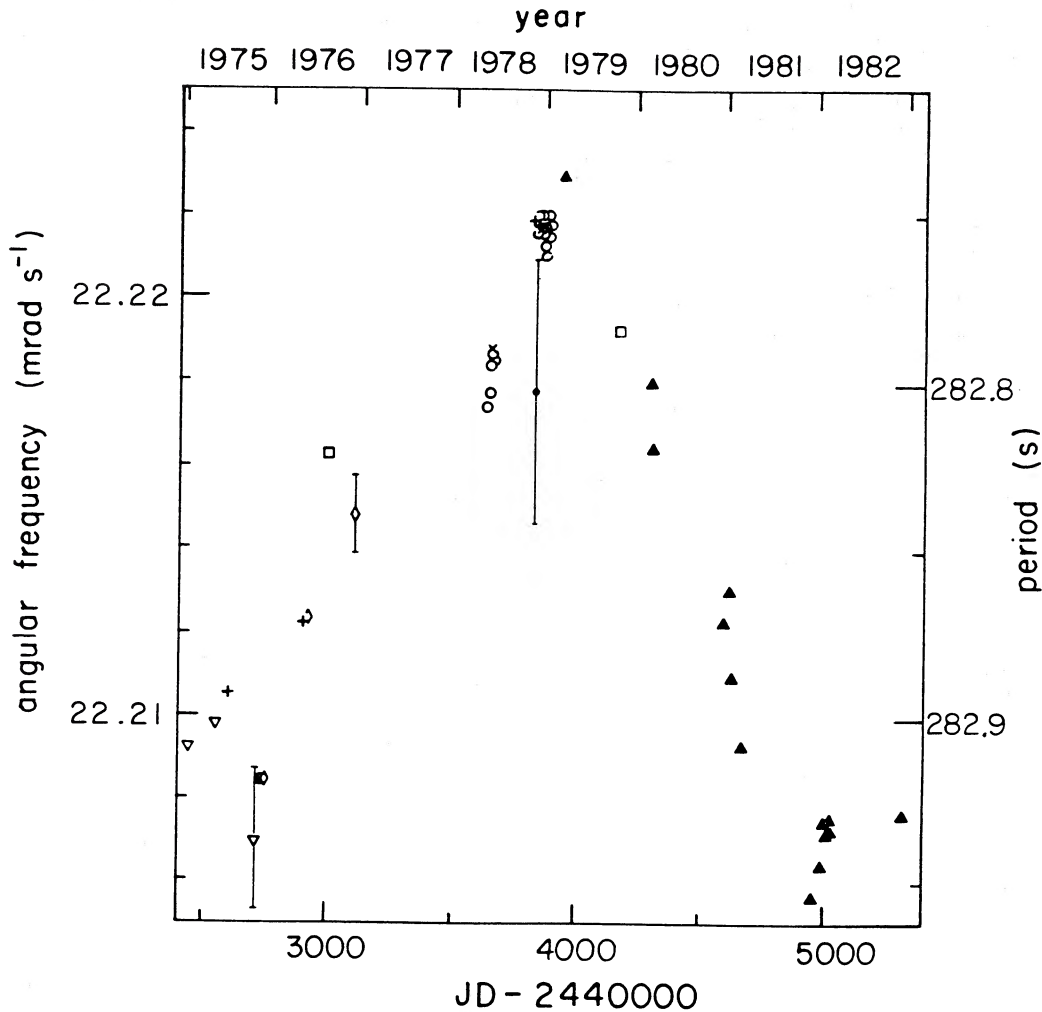
FIG. 2.—Long-term history of the angular frequency of Vela X-1, taken from Tables 1 and 2. The pulse period is also given on the scale at the right, increasing downward. Open inverted triangles are data taken with *Copernicus* and *Ariel 5* (Charles *et al.* 1978); crosses, *SAS 3* (Rappaport, Joss, and McClintock 1976; Rappaport and Joss 1977; Rappaport, Joss, and Stothers 1980); open squares, *COS B* (Ögelman *et al.* 1977; Molteni *et al.* 1982); open diamonds, other *OSO 8* data (Becker *et al.* 1978); open circles, present work; diagonal crosses, other *HEAO 1* data (Bautz *et al.* 1983); filled circle, balloon flight (Staubert *et al.* 1980); filled upright triangles, *Hakucho* (Nagase *et al.* 1984). Vertical bars represent 1 σ confidence intervals and are shown only where they are significantly larger than the symbols. *Hakucho* results have been corrected to the centers of the observing intervals.

1974, 1976). In the remainder of this discussion we will refer to spectra of the form f^{-2r} as describing "*r*th-order" red noise. Thus, the zero-order refers to white noise, the first order to a random walk (red noise), etc.[4] This correspondence between statistical and physical models suggests that computation of the power spectrum of the noise in rotation can be a significant aid in understanding its physical origin.

a) Methodology

The construction of a power density spectrum from the available phase and frequency data is complicated by several factors. Besides the limitations imposed by the data sampling

[4] This characterization of *r*th-order red noise as the *r*th integral of white noise leads to a simple description of the power density spectra of variables which are time integrals of a white-noise variable. Taking a rotating system as an example, the presence of white noise in the angular acceleration, $\ddot{\Omega}$, implies a random walk (first-order red noise) in Ω and a random walk of a random walk (second-order red noise) in pulse phase. Conversely, the variable formed by taking *n* derivatives of the pulse phase will have a spectrum which is *n* orders less red; variables formed by taking derivatives of the white noise variable (the angular acceleration in this example) will have spectra that are blue.

structure, further restrictions are imposed by the nature of the fluctuations in pulse frequency. Visual examination of the pulse record of Figure 2 reveals larger variations on longer time intervals, indicating that the pulse frequency power spectrum is red; the pulse phase spectrum is necessarily even redder. Care must be taken in constructing the spectrum of such fluctuations in order to avoid leakage of power from the lowest accessible analysis frequencies to higher frequencies. Otherwise, the calculated spectrum may not correctly represent the true spectrum (see the discussion by Deeter and Boynton 1982, hereafter DB). The solution to this difficulty proposed by DB works even in the face of moderately nonuniform sampling and involves the computation of carefully band-limited estimates of the noise strength, resulting in a coarse (low frequency-resolution) power spectrum, or "pilot spectrum" in the sense of Blackman and Tukey (1958). Although the discussion of DB is couched for simplicity in terms of power spectra with even-integer power-law exponents, their method applies to power-law spectra in general and even to spectra with significant deviations from a simple power law.

A simplified implementation of this method suggested by

TABLE 2

PREVIOUSLY REPORTED PULSE FREQUENCIES FOR VELA X-1

Data Set[a]	T_{mid}[b] (JD −2,440,000)	Span (days)	Pulse Period[c] (s)	Pulse Frequency[c] (mrad s^{-1})	Ω[d] (prad s^{-2})	Weight[e]	References and Notes
1975 Feb	2449.3	8.8	282.9083 (12)	22.20926 (9)	...	0.33	1
1975 May	2552.3	4.5	282.9010 (37)	22.20984 (29)		0.33	1
1975 Jun–Jul	2600.6	36.4	282.8916 (2)	22.21058 (2)	...	0.33	2
1975 Oct	2713.5	0.5	282.9370 (220)	22.20701 (173)	...	...	3
1975 Nov	2734.7	19.7	282.9190 (12)	22.20842 (9)	−0.3 (0.6)	0.50	4
	2728.4	21.0	282.9108 (12)	22.20907 (9)	−1.0 (0.2)	...	5
1975 Dec	2750.0	10.0	282.9190 (30)	22.20842 (24)	...	0.50	6
1976 May (a)	2900.0	3.0	282.8700 (40)	22.21227 (31)	...	0.30	7
1976 May (b)	2920.0	14.0	282.8690 (30)	22.21235 (24)	...	0.30	6
1976 Aug	3002.5	28.5	282.8190 (20)	22.21628 (16)	0.0 (0.5)	0.30	8
	2997.1	28.0	282.8183 (3)	22.21633 (2)	−0.1 (0.1)	...	5
1976 Nov	3112.0	4.0	282.8380 (120)	22.21478 (94)	...	0.10	6
1978 May	3654.0	3.0	282.7870 (40)	22.21879 (31)	...	...	9
1978 Nov (a)	3824.5	9.0	282.7484 (4)	22.22182 (3)	+0.7 (1.4)	0.13	10
1978 Nov (b)	3836.8	1.0	282.8000 (400)	22.21777 (314)	...	0.01	11
1978 Dec	3850.0	26.0	282.7513 (5)	22.22160 (4)	+0.2 (0.1)	...	12
1979 Mar	3947.4	13.7	282.7350 (9)	22.22288 (7)	+1.5 (0.5)	0.13	13
	3948.1	13.7	282.7337 (9)	22.22298 (7)	+1.7 (0.5)	...	14
1979 Oct	4175.5	35.0	282.7820 (20)	22.21918 (16)	−0.9 (0.4)	1.00	8
	4161.4	35.0	282.7809 (3)	22.21927 (2)	−0.6 (0.1)	...	5
1980 Mar (a)	4308.6	9.8	282.7976 (7)	22.21796 (5)	−1.0 (0.5)	0.50	13
	4308.7	9.8	282.7977 (6)	22.21795 (5)	−0.9 (0.5)	...	14
1980 Mar (b)	4318.1	8.9	282.8176 (8)	22.21639 (6)	−2.4 (0.6)	0.50	13
	4318.1	8.9	282.8174 (7)	22.21640 (5)	−2.3 (0.5)	...	14
1980 Dec	4594.9	9.7	282.8705 (6)	22.21223 (5)	+2.3 (0.5)	0.25	13
	4594.9	9.7	282.8693 (6)	22.21233 (5)	+2.0 (0.5)	...	14
1981 Jan (a)	4617.9	11.1	282.8608 (5)	22.21299 (4)	−3.0 (0.3)	0.25	13
	4617.9	11.1	282.8608 (5)	22.21299 (4)	−2.8 (0.3)	...	14
1981 Jan (b)	4629.4	11.7	282.8874 (6)	22.21091 (5)	−0.2 (0.3)	0.25	13
	4629.3	11.7	282.8872 (6)	22.21092 (5)	−0.3 (0.3)	...	14
1981 Mar	4672.4	12.3	282.9084 (5)	22.20926 (4)	−0.9 (0.2)	0.25	13
	4672.4	12.3	282.9085 (4)	22.20925 (3)	−0.8 (0.2)	...	14
1981 Dec	4958.6	11.0	282.9546 (10)	22.20563 (8)	−1.9 (0.7)	0.25	13
	4958.6	11.0	282.9545 (10)	22.20564 (8)	−1.5 (0.6)	...	14
1982 Jan (a)	4993.8	11.0	282.9450 (9)	22.20638 (7)	+0.1 (0.5)	0.25	13
	4993.8	11.0	282.9451 (7)	22.20638 (5)	+0.8 (0.4)	...	14
1982 Jan (b)	5004.6	9.0	282.9315 (10)	22.20744 (8)	+0.1 (0.7)	0.25	14
1982 Jan (c)	5014.0	9.7	282.9350 (13)	22.20717 (10)	−1.8 (1.0)	0.25	14
1982 Feb	5023.5	7.2	282.9302 (23)	22.20755 (18)	+0.4 (2.1)	0.25	13
	5023.5	7.2	282.9287 (22)	22.20766 (17)	+0.5 (2.1)	...	14
1982 Mar	5031.3	8.5	282.9341 (13)	22.20724 (10)	−2.4 (1.1)	0.25	13
	5031.8	8.5	282.9337 (12)	2220727 (9)	−1.6 (1.1)	...	14
1982 Dec	5320.8	14.7	282.9293 (5)	2220762 (4)	−0.4 (0.3)	1.00	14

[a] Data sets are indicated by the month of observation; two or more sets obtained in the same month are distinguished by a letter in parentheses.

[b] T_{mid} is the center of the data span, usually obtained by averaging the given end-points, and is the nominal epoch for a reported period or frequency based on a linear fit. When $\dot{P}$ or Ω is included in the fit, the epoch for the period should also be specified, and it does not have to correspond to T_{mid}. In some cases, this epoch is substituted for T_{mid}, with T_{mid} given in the notes. *Hakucho* periods (Nagase *et al.* 1982, 1984) were reported for an epoch at the *beginning* of the data span. We have converted these periods to the center of the data span. The uncertainty in the frequency (or period) computed at the midpoint is approximately one-quarter the corresponding uncertainty in the frequency computed at either endpoint.

[c] Uncertainties of 1 σ in the final decimal place for the pulse period and frequency are given in parentheses following the reported and computed values, respectively. In several cases, the listed 1 σ uncertainty has been silently converted from the reported 90% or 95% confidence limit.

[d] Ω has been inferred from $\dot{P}$, whenever the latter is given. Uncertainty of 1 σ follows in parentheses.

[e] Weight used in computing the portion of the power spectrum based on pulse frequencies. Ellipsis indicates that the reported frequency was not used in the calculation of the power spectrum.

REFERENCES AND NOTES.—(1) *Copernicus* (Charles *et al.* 1978). (2) *SAS 3* (Rappaport, Joss, and McClintock 1976). (3) *Ariel 5* (Charles *et al.* 1978). (4) *COS B* (Ögelman *et al.* 1977). The given epoch for the pulse period is listed; T_{mid} is about 5 days later (JD 2,442,740.0). (5) *COS B* (van der Klis and Bonnet-Bidaud 1984). (6) *OSO 8* (Becker *et al.* 1978). The pulse periods have been taken from the caption of their Fig. 3. The plotted value ($P \approx 282.915$ s) for the 1975 Dec set disagrees with the value reported in the figure caption. (7) *SAS 3* (Rappaport and Joss 1977). Data span not given, but has been inferred from a comparison with the uncertainties on the other *SAS 3* data sets. The epoch for this set is not precisely stated, only that it is about 10 months following the 1975 Jun–Jul *SAS 3* observation. (8) *COS B* (Molteni *et al.* 1982). The epoch for the pulse period is not given for either of these data sets, and T_{mid} was taken as an approximate epoch. (9) *HEAO 1*, A-4 (Bautz *et al.* 1983). The given epoch for the pulse period is listed; T_{mid} is perhaps a day later (JD 2,443,655.0). (10) *SAS 3* (Rappaport, Joss, and Stothers 1980). Period is for a linear fit, without $\dot{P}$, so T_{mid} is the appropriate epoch. $\dot{P}$ comes from a separate, quadratic fit for which the period is not reported. (11) Balloon flight (Staubert *et al.* 1980). (12) *HEAO 1*, A-4 (Bautz *et al.* 1983). The given epoch for the pulse period is listed; T_{mid} is about 5 days later (JD 2,443,855.5). (13) *Hakucho* (Nagase *et al.* 1982). See note (b). Based on a simultaneous fit (including orbital parameters) to 11 sets of data. (14) *Hakucho* (Nagase *et al.* 1984). See note (b). Based on a simultaneous fit (including orbital parameters) to 14 sets of data. We took only the three completely new pulse periods from this set in computing the power spectrum, retaining the 11 periods reported in the earlier solution of Nagase *et al.* 1982. The two sets give sufficiently similar values that the choice between them is of no practical consequence.

381

Deeter (1984) employs the discrete analog of Legendre polynomials. As in the earlier work by DB, we estimate the power density at a set of analysis frequencies with octave spacing. Each estimate is an average of the squared amplitudes of selected polynomials applied to subintervals of the data with a duration specified by the analysis frequency. Systematic use of the same degree polynomial from an orthogonal set on every analysis time scale yields a set of local power density estimators that would have identical relative bandpasses if applied to equispaced data. This property of *similarity* (see DB) is crucial for the correct recovery of power-law power spectra with large, negative exponents. The minimum polynomial degree is set by the power-law exponent one reasonably expects in the spectrum and by the level of "protection" desired against contamination of the estimator by low-frequency leakage if the spectrum is redder than expected. For example, if confronted with second-order red noise in pulse phase—as in the Crab pulsar (Boynton and Deeter 1979; Boynton 1981)—one would need to use at least the second-degree polynomial from the orthogonal sequence in order to recover properly the power spectrum of this noise process. However, the cubic polynomial would have to be used in order to provide protection against the possibility that the noise might be slightly redder than second order. In fact, the protection afforded by the cubic polynomial extends to third-order red noise and is used for the analysis presented here.

Although only low-degree polynomials are required for correct recovery of typical red noise, why not choose higher degree functions and thereby achieve improved frequency resolution and increased protection against leakage of low-frequency power? There are several reasons for employing the lowest possible degree consistent with adequate protection against this leakage. First, higher degree polynomials cannot be applied to the small number of data points provided by our observations. Second, higher resolution, even if feasible, would result in less stable estimates. This follows because the largest number of power density estimates at a given analysis frequency is obtained by adopting the lowest usable resolution, thereby achieving the highest stability for each averaged power density estimate. Third, use of the polynomial of the lowest possible degree provides estimates of the power density of the red noise component over the widest possible range of analysis frequencies. The reason is that the highest frequency at which the red noise component stands out above noise is determined by factors unrelated to sampling (see below). Since the polynomial of the lowest possible degree gives a power density estimate with the lowest possible center frequency for a given sampling interval, it provides the broadest frequency coverage. A nominal one octave passband results from choosing the lowest polynomial degree providing one order of protection (e.g., a cubic polynomial on second-order red noise). A polynomial one degree lower (no protection) has a wider passband extending to still power frequencies on the same data set and will result in substantially overlapping power density estimates when applied octave by octave. For a more detailed presentation of these ideas, see DB and Deeter (1984).

As explained below, we use both pulse phase and pulse frequency data in the computation of a power spectrum for Vela X-1. To achieve the same level of protection for the power estimates derived from phases as for those derived from frequencies, it is only necessary to use an orthogonal polynomial of one degree lower for the frequency record than for the phase record. In this way we are able to calculate a single, reasonably homogeneous power spectrum over the full range of time scales covered by both sets of data.

Once the estimators have been constructed, some auxiliary calculations are required. First, we need to calibrate, or "normalize," the power density estimates, and it is convenient to do so in terms of unit-strength red noise of a chosen order. In this paper we employ unit-strength second-order red noise, using the normalization formula (A4) of Deeter (1984).

Second, we need to assign a characteristic center frequency to each estimate. We adopt the median frequency of the estimator passband for this center frequency. Rather than computing the median frequency directly from the specific shape of the passband, we use an approximate method given by Deeter (1984), based on the second central moment of the estimator. For nearly uniform sampling of second-order red noise on a time interval of length L, this frequency is given by $f = 0.92/L$ for one level of protection, and by $f = 0.37/L$ for no protection. This procedure is simple, yet provides a fairer assessment of the median frequency than the inverse of the sampling interval, particularly if the sampling is nonuniform.

Third, it is necessary to characterize both the uncertainty in individual power density estimates and any correlations between estimates that might be present. Each application of a single polynomial estimator to independent data is characterized by a single degree of freedom, so the combination of such estimates to obtain an average power density estimate produces a variable that is distributed as χ^2 with degrees of freedom equal to the total number of estimates combined.

Finally, the contribution of pulse shape noise to each power density estimate is evaluated by propagating the variances in the pulse phase or frequency data into each power density estimate. These variances are based on mean square residuals from local fits to the pulse phases on intervals sufficiently short (0.5 day for the *HEAO 1* data) that pulse shape noise dominates the red noise in pulse frequency. Moreover, a relatively large number of residual degrees of freedom (50 or more) may be obtained for the mean square residual by averaging over many short data segments, yielding power density estimates that have negligible uncertainty when compared to the relatively small number of degrees of freedom provided by the independent low-order polynomial fits to the data. The computed contribution of pulse shape noise to the power density estimates will therefore also have good stability. This procedure does not account for systematic errors in the estimate of the power density in the pulse shape noise, as might be introduced by secular variations in pulse shape, for example. However, any gross deviation from the simple model of white noise in pulse shape variations would be reflected in the structure of the power density spectrum of angular acceleration fluctuations at high analysis frequencies. No evidence for such a deviation is seen in the data analyzed here.

To obtain the coarse power spectrum described above, we first group the data into subsets on a chosen series of time scales, spanning roughly octave intervals, to match the inherent resolution of the estimators. We then compute a power density estimate for each subset on each time scale, utilizing as fully as possible all the available data. The individual power density estimates are then averaged to obtain a single estimate for each time scale having several degrees of freedom. Ideally, we would like to obtain independent power density estimates, which can be guaranteed by choosing the estimators to be nonoverlapping. However, there inevitably will be overlap between estimators on different time scales, and, to ensure effi-

cient use of the data, we allowed some overlap between estimators on the same time scale. As shown by Deeter (1984), the correlation between power density estimates is always positive, so the lack of independence can be accounted for approximately by calculating an *effective* number of degrees of freedom and using this number to characterize the pooled estimate.

The difficulty in obtaining a set of independent power density estimates covering as fully as possible the accessible time scales provided by a discrete, finite time series is common to any attempt to compute a power spectrum from actual observations. In the study of Vela X-1 we also lose some information contained in the pulse phase records by using these data to determine the orbital elements. This effect may be treated as an additional loss of degrees of freedom and is discussed in § III*c*.

b) Experimental Design

Our decision to pursue a statistical representation of the pulse frequency fluctuations in Vela X-1 and of the underlying physical process was made prior to the design of the *HEAO 1* satellite observing program which provided the primary data for this study. Consequently, we were able to design and employ a sampling strategy that would allow a process of statistical inference to be carried out with reasonably efficient use of a limited number of satellite pointings. The inference process we have chosen involves the computation of a power density spectrum of these fluctuations and a subsequent comparison with physically motivated models for such spectra.

From the previous discussion of methodology, it follows that the elements of the design of this experiment are largely forced by the combination of limited sample size and our desire to calculate power densities over as wide a range of analysis frequencies as possible. In order to apply a cubic power density estimator to pulse phase estimates on a given time scale, a minimum of four approximately equispaced satellite observations are necessary. For reasons of symmetry and a desire for some redundancy to protect against possible missed pointings, we chose a five-point sample as a basic unit. Given that successive 12 hr duration pointings had to be separated by at least 1–2 days in order to manage adequately the satellite angular momentum, a spacing of 1.5 days between the midpoints of five successive pointings became the kernel of a sampling pattern.

This pattern was extended to longer time scales by a repeated process of doubling. At each step, a pair of additional pointings is added, one at each end at twice the spacing of the previous five pointings, thereby creating a new quintuplet with twice the span. In this way one increases the sampling interval by one octave for every pair of pointings included. Thus, a total of N pointings (N odd, and greater than or equal to five) can provide symmetric, five-point samples for each of $\frac{1}{2}(N - 5) + 1$ analysis frequencies with octave spacing. Various constraints limited our design to a maximum of 13 pointings, thereby yielding five analysis frequencies with sampling time spans extending from roughly 6 days to 100 days. Shorter time scales can be examined by taking the five pointings at the closest spacing in pairs, giving information on a sampling interval of roughly 2 days, and by utilizing the data structure internal to the 12 hr pointings. On time scales longer than 100 days, information is available as pulse frequencies from other pulse timing studies of Vela X-1 conducted before and after this planned sequence of observations.

Before we undertook these observations, we investigated the

question of statistical inference within the constraints of this sampling pattern by performing Monte Carlo simulations. These numerical simulations verified that the above sampling structure would be adequate to reveal at least the coarse features of the spectrum, despite the low (octave) resolution and relatively low stability of the power density estimates that it provides (1 to 2 degrees of freedom on each time scale).

In such a strongly hierarchical sampling scheme, every pointing, except the first and last, provides essential information on at least two time scales and is therefore crucial to the computation of a useful spectrum. The details of the actual sampling structure achieved are discussed in the following subsections, but the successful completion of the scheme is apparent from the well-spaced power density estimates that were derived.

c) Application to Vela X-1

As stated earlier, we can use the pulse phase estimates presented in Paper I in the computation of the power spectrum only up to the longest available sampling interval provided by the *HEAO 1* and *SAS 3* data. Minor difficulties in implementing the sampling scheme reduced the longest sampling interval to 80 days from the design value of 100 days. For longer intervals, we have used the frequency record drawn from the literature, together with that constructed from our data in 1978 May and 1978 November–1979 January.

As discussed in § III*a*, we need to know the approximate power-law index for the noise in Vela X-1 in order to choose the appropriate degree for the polynomial power density estimator. In particular, white noise in angular acceleration has been established for Her X-1 and the Crab pulsar (Boynton 1981), and we show in this paper that the same description applies to Vela X-1. This behavior is equivalent to second-order red noise in the observed pulse phase and hence requires the use of cubic estimators on the pulse phase record to provide octave bandwidths and one level of protection against the possibility that the noise is even slightly redder. Quadratic estimators should be used on the frequency record to provide the same bandwidths and level of protection. Both of these estimators coincidently give an analysis period, T, defined as the inverse of the analysis frequency, f (the center frequency of the estimator passband defined in § III*a*), that is roughly equal to the time span of the sampling interval to which the estimator is applied. Unless stated otherwise, in the remainder of this paper we will uniformly apply cubic and quadratic estimators to pulse phase and frequency data, respectively. This choice of estimators presumes the result found below for Vela X-1 that the power density at low frequencies is sufficiently close to second-order red noise that the correct power-law exponent will be recovered in the computed spectrum. In fact, this will be correctly recover any power-law spectrum ranging from second-order to third-order noise.

i) Power Density Estimates from the Phase Records

The phases from the 35 days of *OSO 8* data were partitioned into subdivisions on four separate sampling intervals, nominally 35, 17.5, 9, and 4.5 days in length. Each subdivision overlapped up to one-half of the adjacent two on the same time scale; for example, the three subdivisions on the 17.5 day scale start approximately on the 1st, 10th and 19th days of *OSO 8* observations. In this way we obtain one, three, seven, and 15 subdivisions at the four sampling intervals given above. Some of the subdivisions at the two shortest time scales had to be

discarded because irregular sampling made their effective length significantly shorter than the others on the same time scale, leaving one, three, three, and seven usable subdivisions. For each of these remaining subdivisions, we constructed a sequence of orthogonal polynomials of ascending degree, using the third-degree (cubic) polynomial for the power estimator. In constructing the orthogonal sequence, we weighted each point equally, using the observed point variance derived in Paper I. Taking into account the overlap between adjacent estimators, we assigned 1.0, 2.5, 2.8, and 6.3 effective degrees of freedom to the pooled power density estimate derived from each of the four sampling intervals. The data structure is summarized in Table 3.

In contrast to the *OSO 8* data, the *HEAO 1* and *SAS 3* sampling of Vela X-1 was not continuous, but consisted of a specially devised sequence of 0.5 day *HEAO 1* observations separated by intervals from 1.0 to 23 days, followed 17 days later by a 4.5 day continuous observation using *SAS 3*. We were fortunate to acquire a serendipitous *HEAO 1* pointing on 1978 November 30, which has been included also. The design of this hierarchical sampling structure was discussed in § IIIb. Because the planned observing schedule was followed with only minor changes, the pulse phase data can be divided into sampling intervals of nominal length 80, 38, 19.2, 9.6, 5.0, and

TABLE 3

SAMPLING INTERVALS USED IN VELA X-1 POWER SPECTRUM

Nominal Sampling Interval (days)	Intervals Used (JD −2,440,000)	Number of Estimators	Effective d.o.f.
Pulse Frequencies			
2600	2442–5042	1	1.0
1230	2442–3672, 3812–5042	2	2.0
725	2412–3137, 3612–4337, 4307–5032	3	3.0
465	3855–4320, 4165–4630, 4572–5037	3	3.0
320	2442–2762, 2600–2920, 3632–3952	3	3.0
1978 May Pulse Phases			
35.0	3637.5–3672.5	1	1.0
17.5	3637.5–3672.5	3	2.5
9.0	3637.5–3672.5	3	2.8
4.5	3637.5–3672.5	7	6.3
1978 November–1979 January Pulse Phases			
80.0	3813–3893	1	1.0
38.0	3836–3874	1	1.0
19.2	3837.1–3856.3, 3843.2–3862.4, 3849.6–3868.8, 3855.3–3874.5	4	2.5
9.6	3855.7–3865.3, 3858.9–3868.5	2	1.5
5.0	3858.8–3863.8, 3860.3–3865.3, 3888.0–3893.0	3	2.5
2.0	3858.9–3860.9, 3860.4–3862.4, 3861.8–3863.8, 3863.2–3865.3	4	3.6
0.5	3850.0–3850.5, 3855.7–3856.2, 3858.9–3859.4, 3860.4–3860.9, 3861.8–3862.3, 3863.2–3863.7, 3864.7–3865.2, 3867.9–3868.4	8	8.0
0.25	3850.0–3850.5	3	2.5
	3855.7–3856.2	2	2.0
	3858.9–3859.4	2	2.0
	3860.4–3860.9	2	2.0
	3861.8–3862.3	3	2.5
	3863.2–3863.7	2	2.0
	3864.7–3865.2	3	2.5
	3867.9–3868.4	3	2.5

2.0 days, thereby yielding from one to four estimators for each of these time scales (see Table 3). The intervals longer than 2.0 days always span at least four separate pointings, and the shape of the (orthonormal) cubic polynomial is therefore largely determined by the spacing of the pointings and not the data structure within each pointing. On the other hand, the 2.0 day intervals span two 0.5 day pointings separated by a 1 day gap, and the data structure internal to the two pointings becomes important in specifying the polynomial. In addition, eight of the individual 0.5 day observations were sufficiently well covered to provide subintervals with lengths of 0.5 and 0.25 days. For the power density estimator on each sampling interval we again used the cubic polynomial from a sequence of orthogonal polynomials, assigning uncertainties of 0.51 and 0.7 s to the individual determinations of the *HEAO 1* and *SAS 3* phases, respectively. The resulting power density estimates are listed in Table 4.

ii) Power Density Estimates from the Frequency Record

Power density estimates requiring sampling intervals longer than 80 days were based on the pulse frequencies determined from the new data assembled for the present study as well as other, previously published pulse frequencies (see Tables 1 and 2). These frequency estimates were subdivided on a range of intervals from 320 to 2600 days (see Table 3), each subdivision providing the data for one power density estimate. The power density estimates were then obtained from the frequency record in a fashion similar to those obtained from the phase record.

The spacing, density, and weights (inverse variances) of the frequency estimates are quite nonuniform compared to the same properties of the available phase estimates. If we had used the natural weights in constructing these power density estimators, the concentration of a few high-weight frequency estimates (such as provided by the *OSO 8* and *HEAO 1* data) would have rendered the effective data span much shorter than that represented by the selected sampling interval. To alleviate this difficulty, we assigned weights to the frequency estimates, chosen to weight equal time intervals equally. The power density contributed by pulse shape fluctuations was calculated for each estimator by using an appropriate error propagation formula (eq. [39] Deeter and Boynton 1982), and these contributions are listed in Table 4.

iii) Results

Individual power density estimates were constructed by applying the cubic or quadratic polynomial (as appropriate) to the pulse phases or frequencies in each chosen sampling interval to obtain a polynomial coefficient, then squaring this coefficient and dividing by the correct normalization factor for the recovery of second-order red noise. Specification of the distributional properties of the estimates is important in establishing the uncertainties of the individual and pooled estimates. As noted above, each power density estimate formed in this way is distributed as a scaled χ^2 variable with one degree of freedom.

For purposes of plotting and analysis, estimates on the same time scale were averaged to obtain a single, pooled power density estimate. The estimated power density contribution from pulse shape fluctuations was likewise averaged, and the median frequency of each pooled estimate was taken as the average of the median frequencies of the individual estimates.

For some of the power density estimates derived from phases, we used estimators that substantially overlapped. This

TABLE 4

POWER SPECTRUM OF NOISE IN THE DERIVATIVE OF THE PULSE FREQUENCY OF VELA X-1

Nominal Sampling Interval (days)	Analysis Period (1/f) (days)	$\log f$ (Hz)	$\log P_0^a$ (rad² s⁻⁴ Hz⁻¹)	$\log P_t^b$ (rad² s⁻⁴ Hz⁻¹)	Bias in $\log P_t^c$	$\log P_t^d$ (rad² s⁻⁴ Hz⁻¹)	Error in $\log P_t$	Effective d.o.f.	Notes
2600	3200	−8.44	−22.11	−17.44	0.58	−16.86	1.00	1.0	1, 2
1230	1600	−8.13	−21.44	−19.50	0.25	−19.25	0.56	2.0	1, 2
725	900	−7.88	−20.60	−18.06	0.16	−17.90	0.42	3.0	1, 2
465	620	−7.73	−20.67	−18.15	0.16	−17.99	0.42	3.0	1, 2
320	400	−7.54	−20.52	−18.22	0.16	−18.06	0.42	3.0	1, 2
80	82	−6.85	−22.93	−18.60	0.58	−18.02	1.00	1.0	2, 3
36.5	37	−6.50	−20.55	−18.02	0.58	−17.44	1.00	1.0	3
	39	−6.53	−21.87	−18.30	0.58	−17.72	1.00	1.0	3
	38	−6.52	−20.83	−18.14	0.25	−17.88	0.56	2.0	2, 5
18	18	−6.20	−19.33	−18.59	0.20	−18.39	0.48	2.5	4
	20	−6.24	−20.81	−18.27	0.20	−18.08	0.48	2.5	3
	19	−6.22	−19.68	−18.38	0.09	−18.29	0.30	5.0	2, 5
9.6	10.1	−5.94	−19.98	−18.89	0.35	−18.54	0.70	1.5	3
	10.1	−5.94	−19.63	−18.54	0.97	−17.57	1.50	0.67	2, 6
9.0	8.8	−5.88	−18.07	−18.19	0.17	−18.02	0.44	2.8	2, 7
5.0	4.8	−5.62	−18.54	−18.02	0.20	−17.82	0.48	2.5	3
	4.8	−5.62	−18.39	−17.87	0.29	−17.58	0.62	1.76	2, 6
4.5	4.3	−5.57	−17.00	−17.30	0.07	−17.23	0.27	6.3	2, 7
2.0	2.2	−5.27	−17.18	−17.10	0.13	−16.97	0.37	3.6	2, 3
0.5	0.47	−4.61	−15.10	−15.19	0.06	−15.13	0.23	8.0	2, 3
0.25	0.20	−4.24	−13.97	−13.74	0.02	−13.72	0.15	18.0	2, 3

[a] Contribution to the power density estimate from noise induced by fluctuations in the pulse shape.

[b] Total power density, as determined by applying the estimators to the data.

[c] The bias in $\log P_t$ is the difference $\log \langle P_t \rangle - \langle \log P_t \rangle$, and depends on the effective degrees of freedom in the estimate of P_t (see text).

[d] Total power density corrected for bias given in the previous column.

NOTES.—(1) From quadratic estimators applied to the frequency record. (2) Estimate plotted in Fig. 3. (3) From cubic estimators applied to the phase record, 1978 November–1979 January data set. (4) From cubic estimators applied to the phase record, 1978 May data set. (5) Combination of estimates referred to in notes (3) and (4). (6) Previous power density estimate, corrected for loss of information in estimating orbital elements (see text). (7) From cubic estimators applied to the phase record, 1978 May. These power density estimates are dominated by pulse shape noise, and so were ignored in displaying and analyzing the power spectrum. In particular, they were not combined with the corresponding estimates from the 1978 November–1979 January data set.

overlap reduces the effective number of degrees of freedom below the actual number of estimators averaged. For the *OSO 8* data, there was often 50% overlap between adjacent estimators; in such cases we estimate that the total number of degrees of freedom should be reduced by 0.25 per overlap. Likewise, in the *HEAO 1* data there were several cases of about 70% overlap (for 9.6 and 5.0 day sampling intervals), for which the number of degrees of freedom should be reduced by 0.5 per overlap. For the 2 day samples, there is roughly 25% overlap, reducing the effective degrees of freedom by 0.1 per overlap. The corrected number of degrees of freedom expresses in a simple way the amount of information available in the pooled estimates, after accounting for the correlations introduced by sampling.

In addition, there is the extra complication of a reduction in degrees of freedom at analysis frequencies near the orbital frequency and its second harmonic (corresponding to periods of 9.0 and 4.5 days) because information about noise in the data at these frequencies has been "absorbed" in solving for the orbital parameters. In particular, 3 d.o.f. are lost from the entire data set at the orbital frequency in determining the semimajor axis, the orbital epoch, and the orbital period, while 2 d.o.f. are lost at the second harmonic in solving for the eccentricity and the longitude of periapse. The orbital frequencies are closely matched in the power spectrum by power density estimates having analysis periods of 9.6 and 5.0 days, and it is to these estimates that we applied a correction for this loss in degrees of freedom. However, this reduction in degrees of

freedom is necessary only for the power density estimates obtained from the *HEAO 1* data, because the *OSO 8* estimates at these analysis frequencies are dominated by pulse shape noise and are therefore not used in further analysis.

The *HEAO 1* data contributed 37% of the total weight to the orbital solution (Table 5 of Paper I); the simple pro-rated loss in degrees of freedom is therefore $1.11 = 3 \times 0.37$ and $0.74 = 2 \times 0.37$ to the estimates at 9.6 and 5.0 days, respectively. However, the *HEAO 1* data lie close to the weighted center of all the data used to determine the orbital parameters, and only contribute 9% of the weight in determining the orbital period. Taking this factor into account, we reduced the degrees of freedom at 9.6 days by only $0.83 = (2 \times 0.37) + (1 \times 0.09)$, rather than the 1.11 given by simply pro-rating. Thus, rather than assigning 1.5 d.o.f. to the 9.6 day estimate (two estimators minus 0.5 for one overlap) and 2.5 d.o.f. to the 5.0 day estimate (three estimators minus one overlap), we assigned the values of 0.67 d.o.f. (1.5 − 0.83) and 1.76 d.o.f. (2.5 − 0.74), respectively.

This reduction in degress of freedom due to extraction of orbital parameter estimates also necessitates a correction to the estimated power density at these two analysis frequencies because noise power on the corresponding sampling intervals is necessarily absorbed by the least-squares fitting process. Compensation for this absorption is familiar in the related calculation of point variance, wherein the sum of squared residuals is divided by the number of *independent* summands. To compensate for the power absorbed by the orbital solution,

the estimates at 9.6 days and 5.0 days derived from the *HEAO 1* data have been multiplied by 1.5/0.67 and 2.5/1.76, respectively.

The results of these computations are listed in Table 4 and shown in Figure 3. Both present the power density in the second derivative of pulse phase (the derivative of pulse frequency) as a function of the analysis frequency, f. Although the power density estimators have been applied to data expressed as time integrals of the acceleration (pulse frequency and phase), the resulting estimates can be normalized to yield a power spectrum for the noise in pulse angular acceleration (DB). We have chosen angular acceleration as the variable of interest partly because we then see immediately in Figure 3 that it is the variable in which the fluctuations in the pulse frequency of Vela X-1 appear as white noise, at least up to the analysis frequency $f \approx [4 \text{ days}]^{-1}$. At this crossover frequency (cf. Paper I), the pulse shape noise begins to dominate. Angular acceleration is also the *natural* choice since, as explained in § V, the power density in the white-noise variable is not only con-

stant, but numerically equal to the "strength" of the corresponding random walk in pulse frequency. For the purpose of plotting, the *OSO 8* estimates at 35 and 17.5 days have been combined with the *HEAO 1/SAS 3* estimates at 38 and 19.2 days, respectively.

We use a logarithmic rather than a linear plot of the power density estimates, since this shows better that the estimates may be interpreted to exclude power densities that are too small, as well as those that are too large. In addition, we use the logarithm of the analysis frequency for the abscissa, a choice consistent with our use of approximately one octave spacing of the estimates. Additional benefits of this doubly logarithmic representation are that a power-law relationship between P and f appears as a straight line, and estimates with the same number of degrees of freedom have equal weight and equal error bars. Both features are advantageous in fitting for the power-law index.

In Figure 3, the intersection of the vertical and horizontal bars represents the computed power density (ordinate) and the
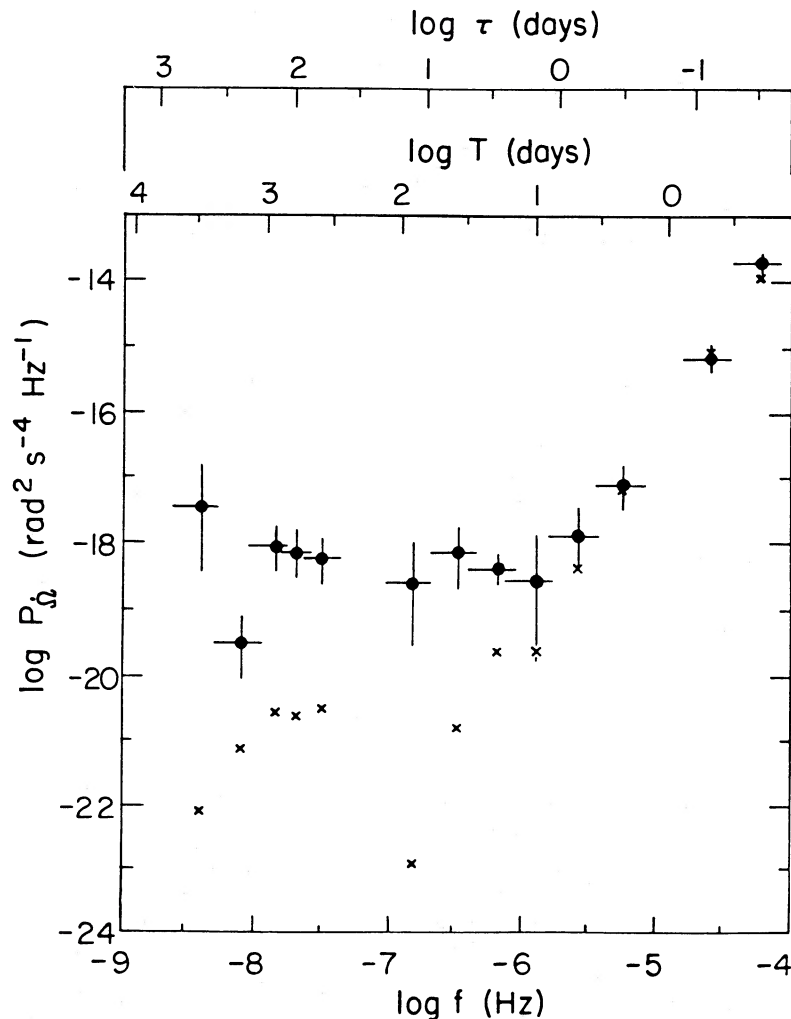

FIG. 3.—Power density of fluctuations in pulse angular acceleration as a function of circular analysis frequency f (*bottom axis*), using power density estimates (not corrected for bias) from Table 4. A sinusoidal variation in Ω with frequency f would produce a feature at period $T = 1/f$ (*lower top axis*), whereas fluctuations in Ω with e-folding time τ (*upper top axis*) would produce a feature at period $T = 2\pi\tau$. The vertical bar on each power density estimate represents the 1 σ confidence interval, based on the effective number of independent estimates contained therein, while the horizontal bar represents the points equivalent to ± 1 σ in the frequency response of each estimator. The diagonal crosses indicate the noise contributed by measurement errors, which are due to variations in the pulse shape.

median frequency (abscissa) of the pooled estimates. The ends of the vertical bars represent the 16% and 84% points[5] on the χ^2 distribution appropriate for the effective degrees of freedom of the power estimate. Similarly, the ends of the horizontal bars represent the 16th and 84th percentiles on the frequency bandpass of the equivalent pooled power density estimator as applied to second-order red noise. The relative width of this function is rather insensitive to the data sampling, so we have uniformly used the equivalent $\pm 1\,\sigma$ points relative to the median frequency, as determined from a computation based on uniform sampling. This is in the spirit of the calibration of median frequency in terms of the half-width of the estimator in the time domain (Deeter 1984).

From the power spectrum presented in Figure 3, it is clear that second-order red noise in pulse phase is a reasonable description of the noise process seen in the Vela X-1 for analysis periods greater than 4 days. It is therefore permissible to drop the one level of protection we used in constructing this initial power spectrum and to repeat the calculation, this time applying quadratic estimators to the pulse phases and linear estimators to the pulse frequencies. The results of this recomputation are shown in Figure 4. Although the frequency

[5] These points are equivalent to the $\pm 1\,\sigma$ points on the Gaussian distribution.

responses of these estimators as applied to second-order red noise are much broader than those of the cubic/quadratic estimators, the resulting power spectrum differs little in overall appearance. This outcome is consistent with the noise interpretation of the fluctuations in pulse frequency. In addition to providing a check on the stability of the power density estimates, this recomputation also makes available a linear estimator applied to pulse frequency, which provides a power density estimate at a median period of 8600 days, substantially longer than the 3200 day median period of the lowest frequency quadratic estimator.

IV. EVALUATION OF THE POWER SPECTRUM

The power density spectra displayed in Figures 3 and 4 provide fairly uniform coverage of the behavior of fluctuations in the derivative of the pulse frequency (the pulse angular acceleration $\dot{\Omega}$) of Vela X-1 over about 13 octaves in analysis frequency. Before proceeding to a quantitative study of the statistical information contained in this representation of the pulse timing data, we use the qualitative features of these spectra to illustrate several general properties of data from this type of source and the limitations imposed by both sampling structure and the nature of the power density estimation process. An understanding of these various features and limi-
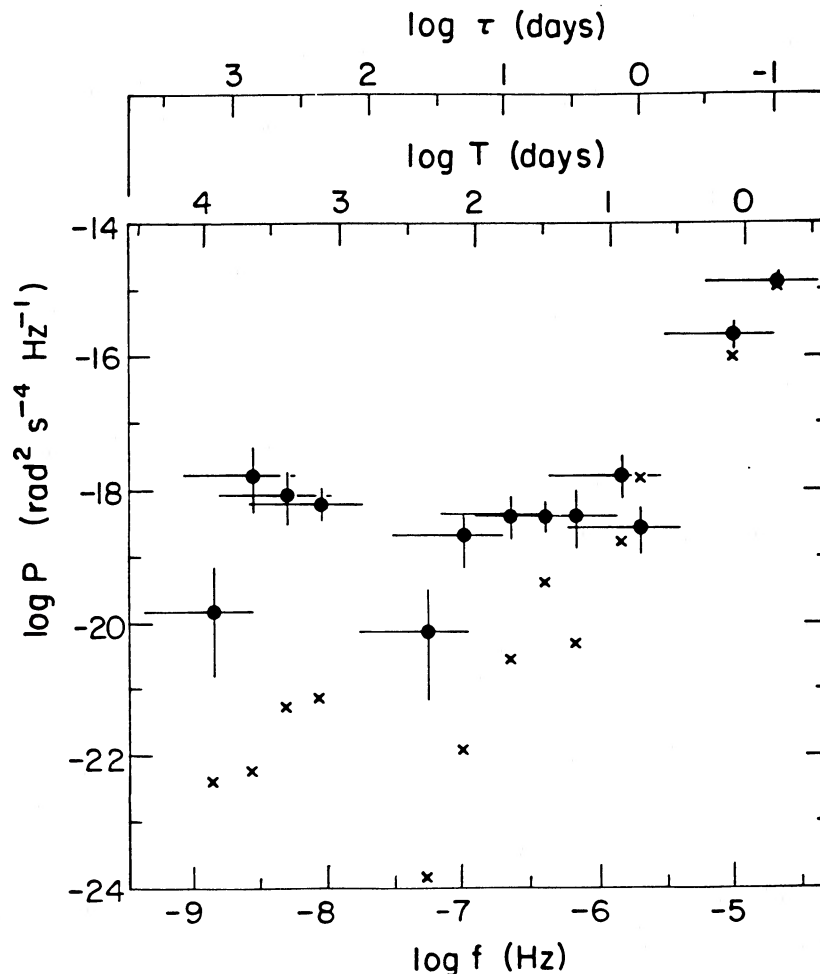

FIG. 4.—Power density of fluctuations in pulse angular acceleration as a function of circular analysis frequency f, based on linear estimators applied to pulse frequencies and quadratic estimators applied to phases. The conventions used in this figure are identical to those used in Fig. 3.

tations serves to guide subsequent analysis and indicates how the experimental design affects the information content of the computed spectrum.

a) Qualitative Assessment

The overall form of the spectra in Figures 3 and 4 is most easily understood as the superposition of two power-law noise processes. The relatively constant power density over the lowest nine octaves indicates a nominally white (f^0) spectrum of fluctuations in the pulse angular acceleration (alternatively describable as second-order red noise in pulse phase). The steep upward slope (approximately f^3; see below) over the remaining four octaves is completely consistent with white noise in pulse phase caused by the fluctuations in pulse shape. The contribution to each power density estimate made by the pulse shape noise (also shown in Figs. 3 and 4) not only fully accounts for the steep rise in the total power density at high frequencies, but also strongly limits our view of the red noise process for analysis periods shorter than about 4 days.

According to the simple argument given in § III and in Paper I (eq. [12]), two factors of f^2 should transform power density spectrum in pulse phase to the spectrum in the pulse angular acceleration shown in Figures 3 and 4. Thus, for uniform sampling of data of fixed quality, one would expect white noise in pulse phase to have an f^4 signature in the power spectrum of the pulse angular acceleration, $P_{\ddot\Omega}(f)$. Over the five highest frequency octaves, the spectrum is derived almost entirely from *HEAO 1* data; while of uniform quality, the hierarchical sampling employed is far from uniform. The sampling density increases as $f = 1/T$ as one proceeds to shorter analysis periods because the sample duration (~ 0.5 day) remains nominally fixed. When viewed in terms of the phase variable, the spectral density, $P_\phi(f)$, for a white process sampled in this way must decrease at high analysis frequencies (thus high sampling density) just as f^{-1}. Consequently, except for unavoidable small irregularities in sampling, upon transforming to $P_{\ddot\Omega}(f)$, one expects to recover the f^3 law observed approximately in Figures 3 and 4. The estimates of the power density of the pulse shape noise over the lowest eight octaves are based on various superpositions of data of markedly inhomogeneous signal-to-noise ratio and sampling density, and thus no obvious pattern is apparent.

We emphasize that the power density estimates for the pulse shape noise (displayed as diagonal crosses in Figs. 3 and 4) are based on the *observed* rms fluctuation in pulse phase on a short time scale (a few hours), which is then presumed to be representative of this noise and is numerically propagated through the chosen polynomial estimators, as if it were white noise, to provide the expected power densities on longer time scales. Thus, the fact that the *measured* power density spectrum at high frequencies coincides with a white-noise model for the *expected* contribution from pulse shape fluctuations verifies both the white-noise character of these fluctuations and that no other significant noise component is present in these data for analysis period shorter than a few days.

For purposes of both statistical and physical inference, we wish to determine the power density spectrum over the widest possible range of analysis frequencies dominated by the process of interest. The preceding qualitative description of the various aspects of the spectrum of fluctuations in angular acceleration of Vela X-1 illustrates the limitations on this range imposed by practical considerations. The "crossover frequency" discussed in Paper I is seen here to be defined by

the intersection of the f^0 and f^3 power laws evident in Figures 3 and 4. For any rotating system exhibiting fluctuations in rotation characterized locally by a power law significantly redder than that describing the contribution induced by pulse shape noise, there must be such a crossover frequency (Lamb 1979). This frequency represents a "soft" upper limit on the analysis frequency for which the redder process (fluctuations in rotation) can be discerned (Boynton and Deeter 1979). The duration of the longest sampling interval places a fundamental limit on the lowest analysis frequency at which power density can be estimated.

The ideas presented here and in Paper I provide some detailed insight to the nature of these limitations. First, the low-frequency limit depends on more than just the duration of the longest sampling interval that can be constructed from the observations of pulse phase or frequency; it also depends on the spectrum of the noise and the nature of the power density estimator chosen. The spectrum shown in Figure 3 extends down to an analysis frequency which is about 20% lower than the value given simply by the inverse of the sampling interval (2600 days). Figure 4 shows a spectrum composed from the same data but with no protection against the low-frequency leakage that would occur if the power law were slightly redder than second-order red noise in pulse phase. We find that the median analysis period of the lowest frequency estimator is about 8600 days, more than 3 times the length of the sampling interval. The nature of this interplay between the character of the noise process and the choice of estimator (which taken together specify the effective passband of the estimator) is discussed in detail by DB and Deeter (1984) and is presented in tabular form in the latter reference.

There are two possibilities for extending the high frequency limit set by the crossover frequency. The substantial reduction (by a factor of $\frac{1}{4}$) in the pulse shape noise achieved by using the pulse filtering method described in Paper I has increased the crossover frequency by about 40%. This increase follows directly from the cube-root scaling of the pulse shape noise power density that applies when the difference in the two power-law exponents is 3. Further reductions in pulse shape noise and still higher crossover frequencies may be possible with more refined techniques (cf. Boynton and Deeter 1986a, b).

The obvious observing-time economy achieved by hierarchical sampling does have some costs. One of these is a loss of information (reduction in degrees of freedom) caused by increased correlation between power density estimators. Another is a displacement of the crossover frequency to a value lower than appropriate to the dense-sampling case. If the central 10 day portion of the high-analysis frequency segment of the hierarchy could have been replaced by continuous monitoring of the source (as was possible within the individual 0.5 day *HEAO 1* pointings), the crossover frequency would have been located at an analysis period of roughly 2.5 days. This apparently rather modest factor-of-two improvement would nonetheless be of considerable help in studying correlations between angular acceleration and X-ray flux using these data (Deeter *et al.* 1988; Lamb *et al.* 1988).

b) Quantitative Assessment

Having discussed the qualitative interpretation of the spectrum shown in Figure 3, we proceed to quantitative evaluations using a series of statistical tests. In applying these tests, we must recognize two more details.

First, broad-band estimators at different frequencies may

have significant correlations if derived from the same set of data. This overresolution causes spectra to appear "too smooth." We estimate that power density estimators spaced at octave intervals and based on uniformly sampled data provide about one-third less information than if the estimators were based on independent data sets. This reduction in effective degrees of freedom is in addition to that caused by applying the estimators to overlapping intervals on the same time scale, a reduction that has already been taken into account above. We have therefore corrected for this effect wherever appropriate in the statistical tests that follow by multiplying all effective degrees of freedom by two-thirds.

Second, in fitting for the power-law index we shall work with log P, whose distribution is different from that of the variable P. Specifically, $\langle \log P \rangle$ is numerically different from $\log \langle P \rangle$. Deeter (1984) has shown that this bias is given by

$$\langle \log P \rangle - \log \langle P \rangle \approx \left[\frac{1}{v} + \frac{1}{v^2} \right] \log e , \qquad (3)$$

where v represents the effective number of degrees of freedom, and the final factor converts the right-hand side from natural to common logarithms. Along with that demonstration, it was shown that the variance in log P may also be expressed approximately in powers of $1/v$:

$$\text{var } (\log P) \approx \left[\frac{2}{v} + \frac{2}{v^2} + \frac{4}{3v^3} \right] (\log e)^2 . \qquad (4)$$

This formal variance gives a measure of the width of the statistical distribution of log P and is the appropriate quantity to use in setting weights in the statistical tests considered below. In the following, the bias $\langle \log P \rangle - \log \langle P \rangle$ and the variance of log P were computed using these formulae.

i) Power-Law Characterization

The average spectral index is the simplest characterization of the power spectrum. To determine the power-law exponent for the spectrum shown in Figure 3, we used ten power density estimates listed in Table 4: five derived from the pulse frequencies, three from the *HEAO 1/SAS 3* pulse phases, and two from the pooled estimates based on *OSO 8*, *HEAO 1*, and *SAS 3* phases. The estimates at 9.0 and 4.5 days that were derived from *OSO 8* phases were not included in the fit because they do not stand out above the pulse shape noise. The estimates at 2.0, 0.5, and 0.25 days that were derived from *HEAO 1* phases were not included for the same reason. The estimates at 17.5 days derived from *OSO 8* phases and those at 9.6 and 5.0 days based on *HEAO 1* phases were corrected for the power density contributed by pulse shape fluctuations and the removal of information that occurred in estimating the orbital parameters before the fit was performed, as discussed earlier.

In performing the fit, each power density estimate was weighted by its inverse variance, uniformly multiplied by two-thirds to take into account the loss of information due to correlations between estimators on different time scales. We found that the spectrum was well fitted by a straight line with a slope of $+0.06 \pm 0.23$, indicating that white noise in pulse angular acceleration (a random walk in pulse frequency or, equivalently, second-order red noise in pulse phase) is an adequate description of the pulse frequency fluctuations and the only acceptable simple noise model. The value for the power-law exponent reported here is slightly different from the value of -0.04 ± 0.22 given in Boynton *et al.* (1984) because of a recon-

sideration of the correction for the information lost in determining the orbit. The change in this value does not affect the conclusions presented by Boynton *et al.* (1984).

Based on this indication that the noise spectrum in pulse angular acceleration is indeed white, we computed the mean power density by averaging the estimates included in the fit, again weighting them with their inverse variances. The mean power density, $(8 \pm 2) \times 10^{-19}$ rad^2 s^{-4} Hz^{-1}, is numerically equivalent to a noise strength $S = R\langle \delta\Omega^2 \rangle$ of 8×10^{-19} rad^2 s^{-3} (see § V). This value, like that for the power law exponent, differs slightly from the noise strength given by Boynton *et al.* (1984) for the reason given above.

ii) Statistical Tests

As a check on the stationarity of the noise process evident in Figure 3, we have compared the average power density calculated for various segments of the data. All of these comparisons rely on the statistical F-test for equality of variance. The comparisons discussed in this subsection are (1) 1978 May versus 1978 December, testing the constancy of the power density in $\dot{\Omega}$ (random walk strength) in time using two disjoint sets of data at analysis periods of 20 and 40 days; (2) power density estimates based on pulse frequencies (at analysis periods between 400 and 3200 days) versus those based on pulse phases (analysis periods of 20 and 40 days), testing the constancy of the power density with analysis period; (3) power density before 1979 January versus after 1979 January, testing the constancy of the power density in time using two disjoint data sets for analysis periods between 400 and 1600 days; and (4) power density at the largest analysis period (3200 days) versus remaining power density estimates, comparing the power spectral density at the largest accessible analysis period with that at shorter periods.

1. 1978 May versus 1978 December.—A test for constancy in time of the power density for analysis periods less than 40 days may be made by comparing the power estimates from the 1978 May and 1978 December data sets. The average density for the 38 and 19.2 day estimates in 1978 December is 5.2×10^{-19} rad^2 s^{-4} Hz^{-1} (all power density estimates will hereafter be given in units of 10^{-19} rad^2 s^{-4} Hz^{-1}), while the average density for the 35 and 19.5 day estimates in 1978 May is 4.6 (corrected for the contribution from pulse shape noise) with about 3 effective degrees of freedom in each power estimate. The ratio, $P_{\text{Dec}}/P_{\text{May}} = 1.13$, is essentially a ratio of variances. Employing an F-test for the equality of numerator and denominator, we find that the average power densities from the two sets are consistent with the same random walk strength, because $F(3, 3)$ is equal to 9.3 at the 95% confidence level.

2. Pulse frequency data versus pulse phase data.—A similar comparison of the power density at analysis periods of 20 and 40 days with the average power density derived from the pulse frequency data (corresponding to analysis periods between 400 and 3200 days) gives a ratio $P_{\text{long}}/P_{\text{short}} = 8.6/4.9 = 1.8$. There are approximately 9 and 6 degrees of freedom in the numerator and denominator, respectively. These two power density estimates are consistent with one another, since $F(9, 6)$ would have to exceed 4.1 to indicate inconsistency at the 95% level.

In § II we noted that the apparent secular trend of the pulse frequency changed from spin-up to spin-down in 1979. An obvious question is whether there is any evidence for a change in the noise in pulse angular acceleration at this time. We therefore tested (3) whether the strength of the noise in $\dot{\Omega}$ derived from the data before 1979 January was significantly

different than the noise derived from the data afterward, and (4) whether the power density at the lowest analysis frequency, which is most sensitive to the change in pulse frequency over the full 2600 day span of the data (corresponding to an analysis period of 3200 days), is significantly different from that at higher analysis frequencies.

3. Power density before and after 1979 January.—Table 3 shows that power density estimates from before and after 1979 January are available at three periods: 1600, 900, and 620/400 days. However, we discard the estimates at 900 days, since they are highly correlated with those at adjacent analysis periods. This leaves one estimate at 1600 days and three at 400 days for the portion of the data prior to 1979 January, and one estimate at 1600 days and three estimates at 620 days for the portion subsequent to 1979 January. Pooling the estimates in each of the two groups, we find that the mean power density was 4.5 before 1979 January, and 5.5 afterwards. The *F*-ratio P_{after}/P_{before} is 1.22 on (4, 4) degrees of freedom. Since the 95% point of $F(4, 4)$ is 6.4, P_{after} does not differ significantly from P_{before}.

4. Power density at the largest analysis period.—In order to test whether the magnitude of the spin-up/spin-down behavior (which dominates the power density on the longest time scale) is compatible with the overall noise strength derived above, we compared the estimated power density at the 3200 day analysis period with the mean of all the estimates at analysis periods shorter than 1600 days (the estimate at 1600 days was excluded because of its large correlation both with the estimate at 3200 days and with the estimate at 900 days). The estimated power density at the largest analysis period is 36.6 (1 d.o.f.), where the mean power density at shorter periods is 7.3 (about 13 d.o.f.). Here, the effective degrees of freedom take into account the correlations between all the estimates, whether at the same period or not. The ratio of the two power densities is 4.9 on (1, 13) degrees of freedom. Since the 95% point of $F(1, 13)$ is 4.7, the power density at the 3200 day analysis period differs from that at the shorter periods at about the 95% confidence level.

In assessing the reliability of any one of the above tests, it should be recognized that the significance of a statistical test depends on the *number* of tests being performed, including those choices implicit in selecting the kind of tests actually performed. In the present study, the significance assigned to the above tests depends on whether the power densities to be compared were selected before the overall appearance of the power spectrum was known or only after the apparent discrepancy in the estimate at the longest time scale was noticed. In the latter case, the significance of the excess power is much less, since with 12 power density estimates there is a high probability that at least one will differ by 2 σ or more. We also note that in the spectrum derived from quadratic-linear estimators (Fig. 4), the power density from the linear estimate on 2600 day sampling interval (corresponding to an analysis period of about 8600 days) is, in fact, one of the smallest. When all the presently available evidence is considered, the power density at the largest analysis period (3200 days and greater) does not appear to differ significantly from that at shorter periods.

V. DISCUSSION

The principal goal of this paper is to provide a phenomenological description of fluctuations in the rest-frame pulse frequency of Vela X-1 for later comparison with physical theories. Inspection of Figures 1 and 2 reveals that frequency fluctua-

tions occur on all time scales accessible with these data. The low-resolution power density spectrum of the observed fluctuations in the time derivative of the pulse frequency shown in Figure 3 suggests two distinct power-law spectral components.

Over the lower nine octaves of the spectrum the power density is roughly constant, indicating a noise process that can be modeled as stationary white noise in the derivative of the pulse frequency. Such a process may also be described as a random walk (first-order red noise) in pulse frequency or a "double random walk" (second-order red noise) in pulse phase (cf. DB). Over the upper four octaves of the spectrum the power density in $\dot{\Omega}$ rises steeply with frequency, with a slope that corresponds to white noise in pulse phase and a strength comparable to that expected from the size and character of the fluctuations in pulse shape that are observed (see Paper I). Although this steeply rising component of the spectrum can provide information on the nature of pulse shape fluctuations, in the present paper our interest centers on the process responsible for the white noise in $\dot{\Omega}$. We therefore focus on the roughly constant component of the power density spectrum of $\dot{\Omega}$ in the discussion that follows.

On theoretical grounds, the spectrum of fluctuations in the derivative of the pulse frequency is expected to be a power law $P(f) \propto f^n$, with $n = 0$ or -2 (Lamb 1979; Lamb, Pines, and Shaham 1978*a, b*). In § IV we reported that fitting a general power-law model to the observed power density spectrum yields a best-fit index $n = +0.06 \pm 0.23$. This result is consistent with white noise in the derivative of the pulse frequency ($n = 0$). In § IV we also summarized the results of a series of statistical tests, each of which is consistent with the hypothesis that the measured spectrum represents white noise. Two of these tests were specifically designed to test whether there was any change in the behavior of the source in 1979 January, when the pulse frequency record seems to suggest a transition from secular spin-up to spin-down, and whether this apparent change in the long-term average of the derivative of the pulse frequency represents behavior distinct from the many changes in the short-term average of this derivative that are present in the record. None of the tests provided evidence for a change in the source properties; all were consistent with the hypothesis that the entire pulse frequency record can be modeled by a single, stationary white noise process. Therefore, in the discussion that follows we adopt white noise in the derivative of the pulse frequency as a simple, plausible, and adequate description of this component of the spectrum.

For a given noise process describing fluctuations in the neutron star rotation rate, the magnitude of the fluctuations in pulse phase, frequency, and higher derivatives of the phase measured on a given time interval are related, and these relations involve the duration τ of the interval. The case in which one of the derivatives of pulse phase exhibits white noise is particularly simple, and yields a set of scaling laws for the dependence on τ of the fluctuation in amplitude of variables that are time integrals of the white-noise variable. In the case of Vela X-1, our results indicate that variations in the pulse frequency time series $\Omega(t)$ [the time integral of $\dot{\Omega}(t)$] can be modeled as a sequence of random steps given by integrating the time series of δ-functions describing white noise in $\dot{\Omega}$. This random walk in $\Omega(t)$ can be characterized by an rms step size $\delta\Omega$ and a step rate R. The resulting mean square frequency excursion in time τ is given by $\langle \Delta\Omega_\tau^2 \rangle = N\delta\Omega^2$, where $N = R\tau$ is the number of steps in the interval and the angle brackets

indicate an ensemble average. This leads to the scaling law,

$$\langle \Delta\Omega_\tau^2 \rangle = R\tau\,\delta\Omega^2 \equiv S\tau \,, \tag{5}$$

where $S = R\delta\Omega^2$ is the strength of the random walk. Equation (5) shows the dependence of the mean square frequency excursion on the length of the interval τ. Any other measure of the size of variations in $\Omega(t)$, such as the expectation of the square of the mean excursion over the interval, necessarily scales with τ in the same way (cf. Cordes 1980; Deeter 1984).

The random walk strength is sufficient to characterize the higher order random walks derived from white noise by integration.[6] Thus, for example, the deviation in pulse phase $\Delta\phi_\tau$ that accumulates from the random walk over an interval of length τ is related to the *mean* excursion in pulse frequency $\overline{\Delta\Omega}_\tau$ over the same interval by $\Delta\phi_\tau = \overline{\Delta\Omega}_\tau \tau$. The ensemble average $\langle (\overline{\Delta\Omega}_\tau)^2 \rangle$ obeys the same scaling law as $\langle \Delta\Omega_\tau^2 \rangle$ (but with a different multiplicative constant), yielding a scaling law for $\langle \Delta\phi_\tau^2 \rangle$,

$$\langle \Delta\phi_\tau^2 \rangle = \langle (\overline{\Delta\Omega}_\tau)^2 \tau^2 \rangle = \tfrac{1}{3} S\tau^3 . \tag{6}$$

The constant factor of $\tfrac{1}{3}$ is determined by more detailed considerations (Cordes 1980; Deeter 1984).

In a similar fashion, the cumulative deviation in Ω can be related to the mean excursion in the white noise variable $\dot\Omega$ by $\Delta\Omega = \overline{\Delta\dot\Omega}\tau$. This leads to the scaling law,[7]

$$\langle (\overline{\Delta\dot\Omega}_\tau)^2 \rangle = S\tau^{-1} . \tag{7}$$

Here the multiplicative constant is unity. This scaling law, which can be rewritten as $S = \langle (\overline{\Delta\dot\Omega}_\tau)^2 \rangle / \tau^{-1}$, states that the random walk strength is numerically equal to the white noise power per unit bandwidth since $\langle (\overline{\Delta\dot\Omega}_\tau)^2 \rangle$ is the frequency-integrated power density and τ^{-1} is the characteristic frequency bandwidth.

According to equation (7), the observed mean square fluctuation in the time derivative of the pulse frequency is expected to be inversely proportional to the averaging time. Inspection of Figures 1 and 2 reveals that typical changes in angular acceleration are indeed much larger on shorter time scales than on longer ones. For example, the rms change in $\dot\Omega$ over the 3 day intervals spanning three consecutive *HEAO 1* pointings is $\sim 3 \times 10^{-12}$ rad s^{-2} compared to $\sim 1.5 \times 10^{-13}$ rad s^{-2} over intervals ~ 1000 days. The observed ratio of ~ 20 in the rms fluctuation at these two time scales is close to the ratio of $1000^{1/2}$ expected for a system exhibiting white noise in $\dot\Omega$.

The scaling law indicated by equation (6) may be used to constrain the physical origin of the fluctuations in the pulse

frequency of Vela X-1. This law specifies that excursions in phase grow arbitrarily large on sufficiently long time scales. Conversely, any process for which excursions in phase are bounded cannot produce a flat noise spectrum for $\dot\Omega$; instead the power density eventually decreases as f^4 toward small analysis frequencies. An example of the latter process is a model in which pulse frequency fluctuations are caused by changes in the direction of the X-ray beam formed at the surface of a neutron star rotating at a constant rate (van der Klis and Bonnet-Bidaud 1984). For this model, the phase excursions are bounded and the rms value cannot exceed ~ 1 rad. On the other hand, for the process described by equation (6), rms excursions larger than 1 rad will typically occur on intervals of duration longer than $\tau = (2/S)^{1/3} \approx 16$ days, using the noise strength S we have derived for Vela X-1. Thus the wandering beam model might explain the spectrum of $\dot\Omega$ at frequencies above $(2\pi \times 16 \text{ days})^{-1} \approx (100 \text{ days})^{-1}$, but it cannot account for the large phase excursions at time scales longer than 16 days and the attendant flat spectrum at analysis frequencies below $(100 \text{ days})^{-1}$. Consequently, we are led to attribute the fluctuations in the angular acceleration of the neutron star crust. Just such fluctuations in the angular acceleration of the crust are expected as a result of variations in the accretion torque acting on the crust (Lamb 1977; Lamb, Pines, and Shaham 1978a, b).

The possibility that changes in the direction of the X-ray beam make a significant contribution to the power density at analysis frequencies well above $(100^d)^{-1}$ cannot be excluded on the basis of the evidence reported here. However, in order for this possibility to be consistent with our results, the power density of fluctuations in the angular acceleration alone would have to decrease with analysis frequency above $(100^d)^{-1}$ in just such a way that the sum of the power densities contributed by fluctuations in the angular acceleration and by fluctuations in the beam direction is equal at these higher frequencies to the power density produced by fluctuations in the angular acceleration of the neutron star crust at lower frequencies. It seems to us difficult to justify the introduction of such complexity when the simple assumption of white noise in the angular acceleration of the crust is adequate to account for all available observations at analysis frequencies for which the power density is not dominated by pulse shape noise.[8] For this reason, in general discussions we have used the phrases "fluctuations in pulse frequency" and "fluctuations in neutron star rotation rate" interchangeably here and in Paper I, understanding that this identification is accurate only for fluctuations at analysis frequencies below the crossover frequency. With the same understanding, we may also identify the rest-frame pulse frequency Ω as the rotation frequency of the neutron star crust, thus providing a physical basis for discussing origins of the observed fluctuations.

The interpretation of the spectrum of $\dot\Omega$ in terms of two distinct noise components was used in Paper I as a basis for calculating uncertainties in the orbital parameters. The power density spectrum (Fig. 3) justifies the inclusion of white noise in $\dot\Omega$ in that error analysis, in addition to the contribution from pulse shape noise. In fact, the average strength of the white noise in $\dot\Omega$ ($\sim 10^{18}$ rad^2 s^{-3}) is more than an order of magnitude larger than the strength of pulse shape noise near the

---

[6] By considering an rth order random walk as the rth time integral of white noise, the question of the role of initial values of the random walk variable and its derivatives in specifying a particular walk is sidestepped. Clearly, if $\dot\Omega$ is white, a particular realization of $\Omega(t)$ requires the specification of an initial value Ω_0. Similarly, a particular realization of the integral of the frequency, i.e., the phase $\phi(t)$, requires specification of two initial values, Ω_0 and ϕ_0. These initial conditions specify a polynomial in time that is to be superposed on the random walk. However, this polynomial is not germane to the statistical characterization of the walk, but only to a particular realization. In fact it is easy to show that the residue from an mth-order polynomial fit to any realization of an rth-order random walk time series scales exactly the same way with time τ as would be calculated for an rth-order random walk with initial values of that variable and its derivatives (through $r - 1$) set to zero (as long as $m > r - 1$). This result was used by Groth (1975) in his early work characterizing the noise in the pulse frequency of the Crab pulsar, was employed by Cordes and Helfand (1980) in their work on many pulsars, and emerges in the formulation of DB as the "moment condition" on power estimators.

[7] This law cannot be generalized to the cumulative excursion in $\dot\Omega$, since this quantity has no meaning for a white noise variable.

[8] Evidence provided by analysis of *Hakucho* observations also supports the interpretation presented here. This evidence will be reported elsewhere (Deeter *et al.* 1988).

orbital frequency ($[9^d]^{-1}$), for the *HEAO 1* data. For other data sets the crossover frequency may be lower than the orbital frequency, so that the contribution from pulse shape noise would then be relatively more important.

VI. CONCLUSIONS

In this paper we have presented estimates of the pulse frequency of the accretion-powered pulsar Vela X-1 over an interval of approximately 3000 days, from early 1975 to late 1982, using both new and previously published observations transformed to the frame of the neutron star using the mean orbit of Boynton *et al.* (1986). We have also estimated the uncertainty in this pulse frequency record caused both by the uncertainty in the pulse phases used to make the frequency estimates and by the uncertainty in the mean orbit used to transform the frequencies to the frame of the neutron star.

Using available pulse phase and frequency records and the methods developed by DB and Deeter (1984), we have calculated a power density spectrum of the fluctuations in the first derivative of the pulse frequency. This spectrum reveals two well-defined components: one consistent with second-order red noise in pulse phase (white noise in $\dot{\Omega}$), which dominates over the lower nine octaves of analysis frequency, and a second component consistent with white noise in pulse phase, which dominates at higher frequencies.

The spectrum of the red noise component implies that the rms fluctuation in the time-average of the first derivative of the pulse frequency increases as $\tau^{-1/2}$ with decreasing averaging interval τ. Just such an increase is found when the rms fluctuation averaged over 3 days is compared with the rms fluctuation averaged over 1000 days. Moreover, the strength of this red noise component implies phase excursions larger than 1 radian for time scales greater than 16 days, ruling out changes in the direction of the X-ray beam relative to the surface of the neutron as the sole cause of the observed pulse fluctuations. On the basis of theoretical expectations of a second-order red noise component in pulse phase and the simplicity of this interpretation relative to alternative hypotheses, we argue that the observed pulse phase fluctuations at frequencies lower than the crossover frequency are caused by fluctuations in the spin rate of the neutron star crust. The observed spectrum then implies that the crust is undergoing a random walk in rotation rate.

The spectrum and strength of the white noise component in pulse phase is consistent with the observed fluctuations in the pulse shape. At frequencies above the crossover frequency, this component obscures the red noise component produced by fluctuations in the spin rate of the neutron star. For studies in which interest centers on the behavior of the neutron star spin rate, this obscuration imposes important limitations on the precision with which the spectrum of spin-rate fluctuations can be estimated above the crossover frequency. The extent of this obscuration can be reduced by appropriate choice of sampling intervals and application of special analysis methods (Boynton and Deeter 1986*a, b*; Deeter and Boynton 1986).

As yet, there is no evidence of any systematic change in the pulse frequency of Vela X-1 with time, in the sense that the variations in frequency on all presently accessible time scales (the nine octaves below the crossover frequency) are consistent with a model in which they are the result of a single, stationary random process. In particular, the apparently opposing secular trends before and after 1979 and the pulse frequency variations observed on much shorter time scales are consistent with the hypothesis that all are the result of stationary white noise in the angular acceleration of the neutron star crust.

Our results place significant constraints on the properties of the neutron star and accretion flow in this system. These constraints will be discussed elsewhere (Lamb *et al.* 1988).

APPENDIX

EFFECT ON FREQUENCY ESTIMATES OF UNCERTAINTIES IN ORBITAL PARAMETERS

To gain insight into how uncertainties in orbital parameters affect the precision of local pulse frequency estimates, we consider the simple situation presented by a circular orbit. We assume that the orbital period is precisely known, so the only uncertainties in the orbit are those in the orbital epoch and semimajor axis. For further simplicity, we treat here only the case where the frequency estimate is computed as the slope between two estimates of pulse phase separated in time; the more general case of fitting a straight line to many phase estimates is mathematically more complex.

First we need an expression for the error in the pulse phase $\Delta\phi$ caused by uncertainty in the orbit. This error can be written as the sum of two conjugate sinusoids at the orbital frequency, namely

$$\Delta\phi = \Delta x \cos \Omega_{\mathrm{orb}}(t - T_{\pi/2}) + \Delta y \sin \Omega_{\mathrm{orb}}(t - T_{\pi/2}) , \qquad (A1)$$

where Ω_{orb} is the orbital frequency and $T_{\pi/2}$ the orbital epoch (the time when the mean longitude equals $\pi/2$). The coefficient Δx is the uncertainty in the projected semimajor axis $x = (\Omega a/c) \sin i$, while the coefficient Δy is a scaled version of the uncertainty in $T_{\pi/2}$,

namely $-x\Omega_{orb} \Delta T_{\pi/2}$ (cf. a similar expression in Deeter, Boynton, and Pravdo 1981). In general, the errors Δx and Δy will be the same order of magnitude; for simplicity we assume they are uncorrelated and have equal variances, that is,

$$\text{var } \Delta x = \text{var } \Delta y = \sigma_x^2 . \tag{A2}$$

The uncertainty in an estimate of the pulse frequency induced by this uncertainty in the orbital parameters is easily computed when the frequency is determined by the slope calculated from two separate estimates of pulse phase. The result is

$$\sigma_\Omega = [\text{var } (\Delta\phi_2 - \Delta\phi_1)]^{1/2}/|t_2 - t_1| . \tag{A3}$$

Here $\Delta\phi_1$ and $\Delta\phi_2$ are the errors in the pulse phase due to the orbital uncertainty specified by equation (A1), at the times t_1 and t_2, respectively. Under the assumptions that Δx and Δy are uncorrelated and have a common uncertainty σ_x, the variance of $\Delta\phi_2 - \Delta\phi_1$ is given by

$$\text{var } (\Delta\phi_2 - \Delta\phi_1) = 2\sigma_x^2(1 - \cos \Omega_{orb} \Delta t) = 4\sigma_x^2 \sin^2 \tfrac{1}{2}\Omega_{orb} \Delta t , \tag{A4}$$

where $\Delta t = t_2 - t_1$. Thus we obtain for the uncertainty in the frequency estimate,

$$\sigma_\Omega = 2\sigma_x \left| \frac{\sin (\Omega_{orb} \Delta t/2)}{\Delta t} \right| = \Omega_{orb} \sigma_x \left| \text{sinc} \left(\frac{\Omega_{orb} \Delta t}{2} \right) \right| . \tag{A5}$$

This result is intuitively plausible; the error in Ω falls off asymptotically as Δt^{-1}, multiplied by a factor depending on the separation of the points in orbital phase. If the two estimates of pulse phase are separated by an integer number of orbital cycles, the contribution σ_Ω to the uncertainty in the frequency estimate vanishes.

REFERENCES

Bautz, M., Howe, S., Gorecki, A., Lang, F., Levine, A., Primini, F., and Lewin, W. H. G. 1983, *Ap. J.*, **266**, 794.
Baym, G., Pethick, C., Pines, D., and Ruderman, M. 1969, *Nature*, **224**, 672.
Becker, R. H., Rothschild, R. E., Boldt, E. A., Holt, S. S., Pravdo, S. H., Serlemitsos, P. J., and Swank, J. H. 1978, *Ap. J.*, **221**, 912.
Blackman, R. B., and Tukey, J. W. 1959, *The Measurement of Power Spectra* (New York: Dover).
Boynton, P. E. 1981, in *IAU Symposium 95, Pulsars*, ed. W. Sieber and R. Wielebinski (Dordrecht: Reidel), p. 279.
Boynton, P. E., and Deeter, J. E. 1979, in *Compact Galactic X-Ray Sources*, ed. F. K. Lamb and D. Pines (Urbana, Il.: UIUC Physics Department), p. 168.
———. 1986a, in *Proc. of the Workshop on Timing Studies of X-Ray Sources*, ed. S. Hayakawa and F. Nagase (Department of Astrophysics, Nagoya University), p. 1.
———. 1986b, in *Proc. of the Workshop on Timing Studies of X-Ray Sources*, ed. S. Hayakawa and F. Nagase (Department of Astrophysics, Nagoya University), p. 13.
Boynton, P. E., Deeter, J. E., Lamb, F. K., and Zylstra, G. 1986, *Ap. J.*, **307**, 545 (Paper I).
Boynton, P. E., Deeter, J. E., Lamb, F. K., Zylstra, G., Pravdo, S. H., White, N. E., Wood, K. S., and Yentis, D. J. 1984, *Ap. J.* (*Letters*), **283**, L53.
Boynton, P. E., Groth, E. J., Hutchinson, D. P., Nanos, G. P., Partridge, R. B., and Wilkinson, D. T. 1972, *Ap. J.*, **175**, 217.
Charles, P. A., Mason, K. O., White, N. E., Culhane, J. L., Sanford, P. W., and Moffat, A. F. J. 1978, *M.N.R.A.S.*, **183**, 813.
Cordes, J. M. 1980, *Ap. J.*, **237**, 216.
Cordes, J. M., and Helfand, D. J. 1980, *Ap. J.*, **239**, 640.
Deeter, J. E. 1981, Ph.D. thesis, University of Washington (Ann Arbor: University Microfilms).
———. 1984, *Ap. J.*, **281**, 482.
Deeter, J. E., and Boynton, P. E. 1982, *Ap. J.*, **261**, 337 (DB).

———. 1986, in *Proc. of the Workshop on Timing Studies of X-Ray Sources*, ed. S. Hayakawa and F. Nagase (Department of Astrophysics, Nagoya University), p. 29.
Deeter, J. E., Boynton, P. E., and Pravdo, S. H. 1981, *Ap. J.*, **247**, 1003.
Deeter, J. E., Boynton, P. E., Lamb, F. K., Shibazaki, N., Hayakawa, S., and Nagase, F. 1988, in preparation.
Groth, E. J. 1975, *Ap. J. Suppl.*, **29**, 453.
Lamb, F. K. 1977, in *Proc. 8th Texas Symposium on Relativistic Astrophysics* (*Ann. N.Y. Acad. Sci.*, **302**, 482).
———. 1979, in *Proc. HEAO Science Symposium*, ed. C. Daily and W. Johnson (NASA CP-2113), p. 223.
Lamb, F. K., Pines, D., and Shaham, J. 1974, talk presented at the 7th Texas Symposium on Relativistic Astrophysics (unpublished).
———. 1976, in *X-Ray Binaries, Proc. Goddard Conference*, ed. E. Boldt and Y. Kondo (NASA SP-389), p. 141.
———. 1978a, *Ap. J.*, **224**, 969.
———. 1978b, *Ap. J.*, **225**, 582.
Lamb, F. K., Zylstra, G., Boynton, P. E., and Deeter, J. E. 1988, in preparation.
Molteni, D., Rapisarda, M., Re, S., and Robba, N. R. 1982, *Astr. Ap.*, **111**, 365.
Nagase, F., *et al.* 1982, *ISAS Research Note 178* (Tokyo: ISAS).
Nagase, F., *et al.* 1984, *Ap. J.*, **280**, 259.
Ögelman, H., Beuermann, K. P., Kanbach, G., Mayer-Hasselwander, H. A., Capozzi, D., Fiordilino, E., and Molteni, D. 1977, *Astr. Ap.*, **58**, 385.
Rappaport, S., and Joss, P. C. 1977, *Nature*, **266**, 683.
Rappaport, S., Joss, P. C., and McClintock, J. E. 1976, *Ap. J.* (*Letters*), **206**, L103.
Rappaport, S., Joss, P. C., and Stothers, R. 1980, *Ap. J.*, **235**, 570.
Scargle, J. D. 1982, *Ap. J.*, **263**, 835.
Staubert, R., Kendziorra, E., Pietsch, W., Reppin, C., Trümper, J., and Voges, W. 1980, *Ap. J.*, **239**, 1010.
van der Klis, M., and Bonnet-Bidaud, J. M. 1984, *Astr. Ap.*, **135**, 155.

P. E. Boynton and J. E. Deeter: Department of Astronomy, University of Washington, Seattle, WA   98195

F. K. Lamb: Department of Physics, University of Illinois at Urbana-Champaign, Urbana, IL   61801

G. Zylstra: Department of Physics, Washington University, Box 1105, St. Louis, MO   63130